

A Bayesian Generalized Bridge Regression Approach to Covariance Estimation in the Presence of Covariates

Christina Zhao

School of Statistics
University of Minnesota
zhaox684@umn.edu

Ding Xiang

Liberty Mutual Insurance
xiang045@alumni.umn.edu

Galin L. Jones

School of Statistics
University of Minnesota
galin@umn.edu

Adam J. Rothman

School of Statistics
University of Minnesota
arothman@umn.edu

June 4, 2024

Abstract

A hierarchical Bayesian approach that permits simultaneous inference for the regression coefficient matrix and the error precision (inverse covariance) matrix in the multivariate linear model is proposed. Assuming a natural ordering of the elements of the response, the precision matrix is reparameterized so it can be estimated with univariate-response linear regression techniques. A novel generalized bridge regression prior that accommodates both sparse and dense settings and is competitive with alternative methods for univariate-response regression is proposed and used in this framework. Two component-wise Markov chain Monte Carlo algorithms are developed for sampling, including a data augmentation algorithm based on a scale mixture of normals representation. Numerical examples demonstrate that the proposed method is competitive with comparable joint mean-covariance models, particularly in estimation of the precision matrix. The method is also used to estimate the 253×253 precision matrices of two classes of spectra extracted from images taken by the Hubble Space Telescope. Some interesting structural patterns in the estimates are discussed.

1 Introduction

The simultaneous modeling of multiple numerical response variables is a fundamental problem. A Bayesian shrinkage estimation framework is proposed under the following model. Let Y_i be a q -variate response random vector and $X_i \in \mathbb{R}^p$ be the associated covariate vector for the i th subject, and let $B \in \mathbb{R}^{p \times q}$ be the regression coefficient matrix. Define ε_i to be a q -variate latent random vector with zero mean and positive definite, diagonal covariance matrix D and $L \in \mathbb{R}^{q \times q}$ to be a lower triangular matrix with ones on its diagonal. The distribution of Y_i is described by the multivariate linear model

$$Y_i = B^\top X_i + L\varepsilon_i, \quad i = 1, \dots, n. \quad (1)$$

Denote the covariance matrix of the Y_i 's by Ω^{-1} .

Although several frequentist approaches for simultaneous estimation of (B, Ω) in this multivariate linear model have been proposed (Rothman et al., 2010; Lee and Liu, 2012; Cai et al., 2013), there is limited work in this setting from a Bayesian perspective. Several approaches focus on structure learning for Ω and either provide only an estimate of its sparsity structure (Bhadra and Mallick, 2013; Bottolo et al., 2021) or relax the positive definite constraint in estimation (Samanta et al., 2022). Methods that both estimate Ω itself and preserve the positive definite constraint include the multivariate spike-and-slab LASSO (mSSL) (Deshpande et al., 2019) and the horseshoe-graphical horseshoe (HS-GHS) (Li et al., 2021). Both mSSL and HS-GHS extend priors used in sparse univariate-response linear regression to the multivariate case. mSSL specifies spike-and-slab lasso priors (Ročková and George, 2018) on each element of B and the off-diagonal elements of Ω , while HS-GHS uses the horseshoe prior (Carvalho et al., 2010). The prior on Ω is then truncated to the space of positive definite, symmetric matrices. Li et al. (2021) consider full posterior inference, but Deshpande et al. (2019) only consider computation of the posterior mode.

Full posterior inference on (B, Ω) using a novel penalized regression prior is proposed here. Whereas use of the ridge and lasso regression penalties would require the practitioner to consider penalty selection in model fitting, the proposed prior addresses this nuisance parameter using a type of model averaging approach. Furthermore, the range of the penalty is extended beyond the commonly used range of $[1, 2]$. Allowing penalty values less than 1 encourages sparsity when appropriate, while values greater than 2 improve performance in dense settings. The proposed generalized bridge (GBR) prior also uses local shrinkage parameters. This results in a local-global interpretation and leads to the same sort of tail-robustness properties enjoyed by the horseshoe (Carvalho et al., 2010). In estimation and prediction, the GBR prior is competitive with the horseshoe and the spike-and-slab lasso (Ročková and George, 2018).

When extending the GBR prior to multivariate linear regression, estimation of Ω is first converted to estimation of a sequence of q autoregressions (Pourahmadi, 1999), and the GBR prior is specified in an element-wise fashion for B and the coefficients of the autoregressions. The connection between Ω and autoregression is now described. For ease of exposition, let $\mu \in \mathbb{R}^q$ and consider the following special case of equation (1), with a single Y and ε :

$$Y = \mu + L\varepsilon. \quad (2)$$

Define $T = L^{-1}$, which is also lower triangular with ones on its diagonal. The modified Cholesky decomposition is given by

$$\Omega = T^\top D^{-1}T. \quad (3)$$

Since $\varepsilon = T(Y - \mu)$ express its j th row equality as

$$Y_j = \mu_j - T_{j,1}(Y_1 - \mu_1) - \cdots - T_{j,j-1}(Y_{j-1} - \mu_{j-1}) + \varepsilon_j, \quad j \in \{2, \dots, q\},$$

which is the linear regression of Y_j on Y_1, \dots, Y_{j-1} . Let (\hat{T}, \hat{D}) be an estimator of (T, D) based on fitting these q regressions. The corresponding precision matrix estimator is $\hat{\Omega} = \hat{T}^\top \hat{D}^{-1} \hat{T}$, which is guaranteed to be positive definite and symmetric, but is not invariant to permutations of the variables. As a result, it is more suited to applications where Y has a natural ordering, such as longitudinal or spatial data (Wu and Pourahmadi, 2003; Kidd and Katzfuss, 2022), though it has been applied to financial returns data for computing the covariance matrix for q assets (Carvalho et al., 2010; Gramacy and Pantaleo, 2010). Methods have been proposed to address the ordering issue – see for example Kang and Deng (2020) and Zheng et al. (2017) – but a natural ordering of the variables is assumed to be available here.

A related idea is neighborhood selection (Meinhausen and Bühlmann, 2006), which estimates Ω by regressing each element of Y on all other elements. This results in a pseudolikelihood. Although the resulting estimator is permutation invariant, it is not guaranteed to be positive definite or symmetric (Yuan and Lin, 2007). Jalali et al. (2020), Samanta et al. (2022), and Williams et al. (2018) proposed Bayesian methods taking this approach.

Under the assumption that ε is Gaussian, Bayesian approaches using the modified Cholesky decomposition have considered a variety of univariate-response regression priors. Daniels and Pourahmadi (2002) used conjugate priors without making sparsity assumptions. Many others first impose sparsity and then specify a multivariate normal prior on the coefficients conditional on the sparsity pattern. Lee et al. (2019) and Smith and Kohn (2002) allow an arbitrary sparsity pattern, while Kidd and Katzfuss (2022) and Lee and Lin (2023) assume a banded structure for T . Lee and Lee (2021) also assume

a banded structure but specify a flat prior on the coefficients. Surprisingly, penalized regression priors have received little attention. [Gramacy and Pantaleo \(2010\)](#) consider ridge and lasso priors, but penalized regression approaches are often considered under a frequentist paradigm ([Huang et al., 2006](#); [Levina et al., 2008](#)). Additionally, many of these methods focus on covariance estimation and estimate μ with the sample mean; among the methods mentioned here, only [Daniels and Pourahmadi \(2002\)](#) and [Smith and Kohn \(2002\)](#) also consider mean estimation in the presence of covariates.

The proposed model makes use of the regression framework provided by the modified Cholesky decomposition for estimating Ω while allowing μ to depend on the value of predictors, as described by equation (1). The resulting posterior distribution is analytically intractable in the sense that closed-form expressions for posterior quantities of interest are not available. Two Markov chain Monte Carlo (MCMC) algorithms are developed for sampling from the posterior. The first is a standard component-wise algorithm that can accommodate values of the penalty parameter greater than 2. The second is a data augmentation algorithm that, although unable to allow penalty values greater than 2, is computationally more efficient, reducing the number of required Metropolis-Hastings updates from $pq + q(q - 1)/2 + 2$ to 2.

The data augmentation algorithm uses a scale mixture of normals (SMN) representation of the exponential power distribution ([West, 1987](#)) to augment the posterior conditionals of the elements of B and the lower triangular matrix T . This allows sampling using multivariate normal distributions, even when $p > n$ and $q > n$, without changing the posterior conditionals of the other parameters. While standard calculations suffice for demonstrating this for T , sampling from a multivariate normal distribution for B in the $p > n$ case requires a transformation that uses T and the $p \times p$ orthonormal matrix of the singular value decomposition (SVD) of the covariate matrix X . Two sampling strategies for the multivariate normal distribution are considered: the approach of [Bhattacharya et al. \(2016\)](#) is used when the dimension of the normal distribution to be sampled is greater than the sample size, and the approach of [Rue \(2001\)](#) is used otherwise.

Due to the computational considerations in the development of the data augmentation algorithm, the proposed model can be fitted to datasets with large n that the available implementation of HS-GHS is unable to fit due to memory constraints. The data example in Section 6 uses spectra extracted from images obtained by the Hubble Space Telescope. These spectra have length $q = 253$, and the analysis compares the precision matrices of spectra with and without emission lines. The training sample for the spectra without emission lines had a sample size of $n = 90,670$, and there are no covariates. The HS-GHS algorithm requires inversion of an $nq \times nq$ matrix to sample the mean structure, and for this data example, 128 gigabytes (GB) of random-access memory (RAM) was insufficient for completing this operation for a single iteration of the algorithm. On the other hand, because $p = 1 < n$ and $q < n$, the proposed data augmentation algorithm pre-computes

products involving matrices with n rows, so that the largest matrix required is $q \times q$. As a result, 16 GB of RAM was sufficient for 5000 iterations of the data augmentation algorithm in this example.

The remainder proceeds as follows. Section 2 develops the GBR prior for univariate-response regression, and Section 3 extends it to estimation of (B, Ω) to construct the generalized mean-covariance bridge (GMCB) prior. Point estimates and the sampling algorithms are discussed in Section 4. Estimation performance is compared to other joint mean-covariance methods in Section 5, and GMCB is demonstrated on emission spectra in Section 6. Concluding remarks are offered in Section 7.

2 The Generalized Bridge Prior

The modified Cholesky decomposition transforms the estimation of Ω into a sequence of univariate-response regression problems. A penalized regression approach that allows elimination of the nuisance parameters through the use of marginal densities for inference is developed in this setting, before considering its extension to the multivariate linear model in Section 3.

When considering penalized regression methods, many can be described by a common framework. Let $\|\cdot\|_2$ denote the Euclidean norm. If Y is an $n \times 1$ vector of centered responses, X is an $n \times p$ standardized matrix of covariates, and β is a $p \times 1$ vector of regression coefficients, for fixed $\alpha > 0$ and $\lambda > 0$, the frequentist penalized regression estimate is the solution to

$$\arg \min_{\beta} \|Y - X\beta\|_2^2 + \lambda \sum_{j=1}^p |\beta_j|^\alpha. \quad (4)$$

Choices of $\alpha = 1$ and $\alpha = 2$ correspond to the frequentist lasso (Tibshirani, 1996) and ridge (Hoerl and Kennard, 1970) estimates, respectively. Values of α other than 1 and 2 in $(0, 2]$ correspond to the frequentist bridge estimate (Frank and Friedman, 1993), though values of $\alpha < 1$ have been limited in application due to non-convexity.

Bayesian penalized regression priors may be constructed so that the frequentist estimates are the posterior modes. If I_n denotes the $n \times n$ identity matrix, a standard Bayesian formulation of penalized regression models assumes

$$Y|X, \beta, \sigma^2 \sim N(X\beta, \sigma^2 I_n),$$

$$\nu(\beta|\lambda, \alpha, \sigma^2) = \left(\frac{\alpha \lambda^{1/\alpha}}{2^{1/\alpha+1} (\sigma^2)^{1/\alpha} \Gamma(1/\alpha)} \right)^p \exp \left\{ -\frac{\lambda}{2\sigma^2} \sum_{j=1}^p |\beta_j|^\alpha \right\}. \quad (5)$$

For fixed (λ, α) and $\nu(\sigma^2) \propto 1/\sigma^2$, the marginal posterior distribution of β is characterized

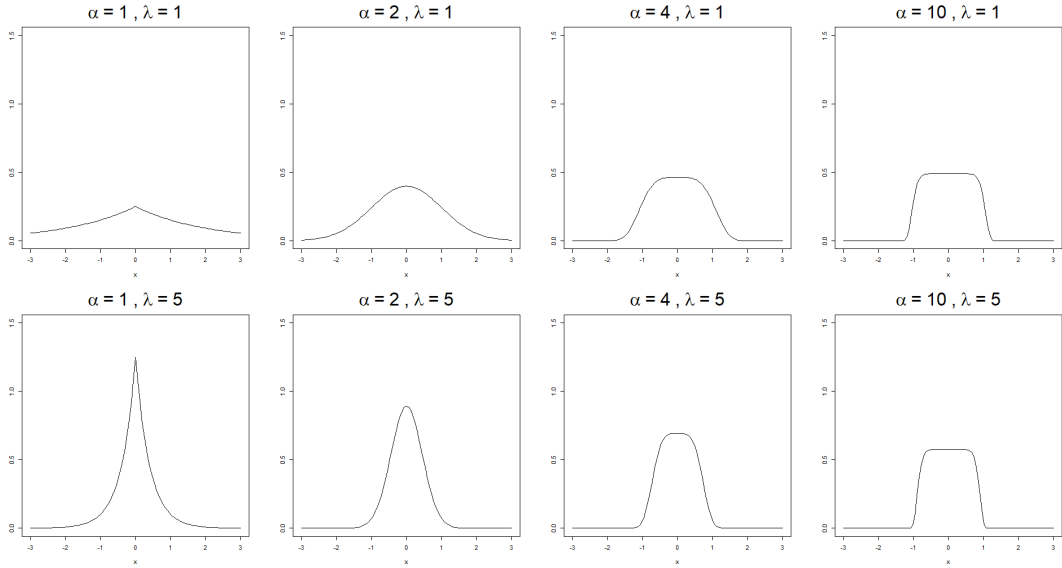


Figure 1: Exponential power prior on β_j for different values of λ and α when $\sigma^2 = 1$.

by

$$q(\beta|Y) \propto \left[\|Y - X\beta\|_2^2 + \lambda \sum_{j=1}^p |\beta_j|^\alpha \right]^{-\left(\frac{n}{2} + \frac{p}{\alpha} + 1\right)}, \quad (6)$$

and hence the mode of this distribution is the solution to equation (4).

Equation (6) requires a choice of λ and α . While λ is often modeled with a prior or selected through methods such as cross-validation or empirical Bayes approaches, similar treatment of α is not widespread. Polson et al. (2014) consider a prior for $\alpha \in (0, 1)$, but other approaches fix α at a pre-selected or estimated value (Park and Casella, 2008; Mallick and Yi, 2018; Armagan, 2009; Griffin and Hoff, 2020), despite the optimal choice of α varying based on the nature of the unknown β (Tibshirani, 1996; Fu, 1998). As shown in Figure 1, smaller values of α accommodate large signals and sparsity, while larger values accommodate small non-zero signals. For estimating an unstructured covariance matrix, it is necessary to accommodate both sparse and dense settings, which is difficult when α is a fixed value.

Figure 1 also highlights the role of λ in the prior's behavior in sparse settings, where small α is preferred. The value of λ must be large enough to shrink noise sufficiently but also small enough to avoid overshrinking large signals. When a single value of λ is specified for all β_j , as in standard penalized regression priors, this can lead to sub-optimal performance; Carvalho et al. (2010) discuss this trade-off for the case $\alpha = 1$. The proposed prior addresses these limitations by using a prior for $(\lambda, \alpha) \in (0, \infty)^p \times [k_1, k_2]$, where $0 < k_1 \leq 1$ and $2 \leq k_2$. Allowing k_1 to be less than 1 will encourage sparsity when appropriate, while allowing k_2 to be larger than 2 will yield improved performance in dense settings. Replacing the scalar λ with a p -dimensional vector allows for differing

shrinkage in estimating each β_j .

As in the standard Bayesian formulation of penalized regression, the proposed prior assumes

$$Y|X, \beta, \sigma^2 \sim N(X\beta, \sigma^2 I_n).$$

A proper conjugate prior $\sigma^2 \sim \text{IG}(a, b)$ is assumed, and the prior on β is

$$\nu(\beta|\lambda, \alpha, \sigma^2) = \left(\frac{\alpha}{2^{1/\alpha+1}(\sigma^2)^{1/\alpha}\Gamma(1/\alpha)} \right)^p \left(\prod_{j=1}^p \lambda_j \right)^{1/\alpha} \exp \left\{ -\frac{1}{2\sigma^2} \sum_{j=1}^p \lambda_j |\beta_j|^\alpha \right\}.$$

The only difference from equation (5) is that each β_j is assigned a parameter $\lambda_j > 0$. Routine calculation shows that $\mathbb{E}(\beta_j|\lambda_j, \sigma^2, \alpha) = 0$ and

$$\text{Var}(\beta_j|\lambda_j, \sigma^2, \alpha) = \frac{\Gamma(3/\alpha)}{\Gamma(1/\alpha)} \left(\frac{\lambda_j}{\sigma^2} \right)^{-2/\alpha} 4^{1/\alpha}.$$

Hence the variance is a decreasing function of λ_j . If λ_j is small, larger values of β_j are likely but if λ_j is large, smaller values of β_j are likely. This suggests a way to incorporate a spike-and-slab prior through the prior for λ_j , with

$$\lambda_j \sim \frac{1}{2} \text{Gamma}(e_1, f_1) + \frac{1}{2} \text{Gamma}(e_2, f_2).$$

The hyperparameters are chosen so that one component of the mixture has a small mean and variance while the other can have a relatively large mean and variance.

Finally, a prior for α needs to be specified. Notice that unlike λ_j , which controls shrinkage for an individual β_j , this parameter is common to all of the β_j . If one wants to maintain the analogy with the frequentist methods in equation (4), the prior for α can be specified as a mixture of three components, where each represents the analyst's assessment of the relative importance of lasso, bridge, and ridge. Empirical work for such a mixture prior indicated that different choices for the mixture parameters yield similar estimation and prediction. This motivated consideration of a uniform distribution for α which has been found to work well, especially since extending the range of α appears to be impactful. Therefore it is assumed that

$$\alpha \sim \text{Unif}(k_1, k_2), \quad 0 < k_1 \leq 1, \quad 2 \leq k_2.$$

The prior obtained for β by marginalizing over λ , α , and σ^2 is referred to as the generalized bridge (GBR) prior.

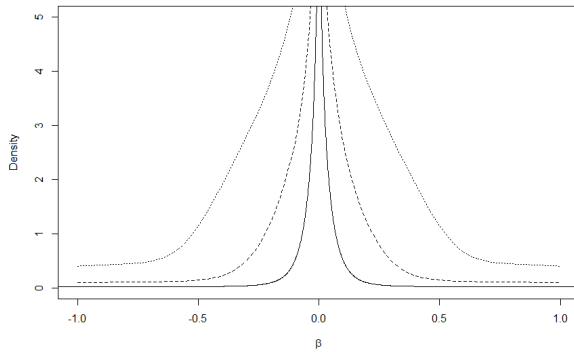


Figure 2: GBR density for $k_2 = 2$ (solid), $k_2 = 4$ (dashed), and $k_2 = 8$ (dotted) when $k_1 = 1$ and $(e_1, f_1, e_2, f_2) = (0.1, 1, 2, 0.01)$.

2.1 Hyperparameter Specification

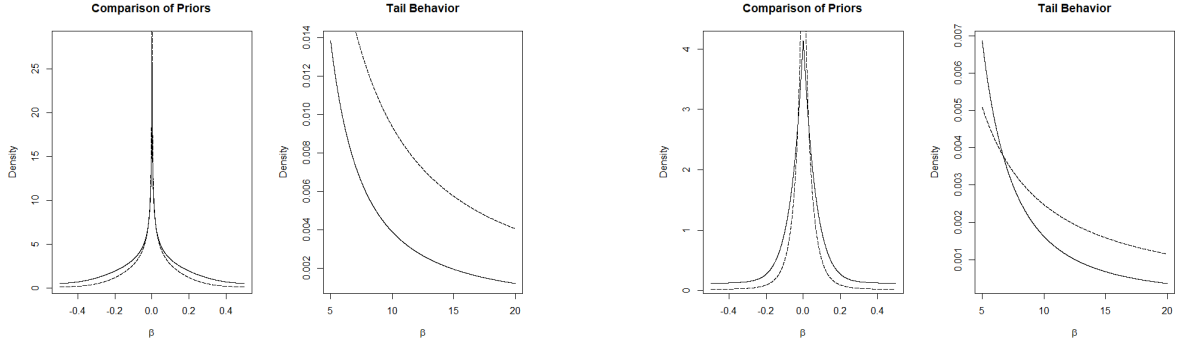
Consider the effect of the hyperparameters on the GBR prior’s density for a single regression coefficient when $\sigma^2 = 1$. Figure 2 shows that larger values of k_2 increase both the mass assigned to the neighborhood around zero and the size of that neighborhood. The value of k_1 has a minimal effect on these aspects of the density and instead determines the value at zero, with smaller values resulting in a taller spike (Table 1). Thus larger values of k_2 are more suitable for dense settings, while small values of k_1 encourage sparsity.

Table 1: Value of GBR density at zero for different values of k_1 when $k_2 = 2$ and $(e_1, f_1, e_2, f_2) = (0.1, 1, 2, 0.01)$.

k_1	$\nu(0)$
0.01	5.105×10^{166}
0.1	7.068×10^{14}
0.5	151.337
1	7.851

Compared to k_1 and k_2 , the values of e_1 , f_1 , e_2 , and f_2 have more moderate effects on the density. Recall that these hyperparameters are specified so that the mean and variance of the first component of the prior on λ_j are small and the mean and variance of the second component are large. Larger values of e_1 and smaller values of f_1 result in more mass near zero. Smaller values of f_2 result in more mass concentrated at zero. The effects of e_2 are most prominent, with values of $e_2 \leq 1$ resulting in flatter densities.

Empirical work for the scenarios described in Section 5 suggests that the hyperparameters $(e_1, f_1, e_2, f_2) = (0.1, 1, 2, 0.01)$ work well for sparse settings and $(e_1, f_1, e_2, f_2) = (1, 1, 40, 0.5)$ work well for dense settings. Figure 3a compares the two densities with $(k_1, k_2) = (0.5, 4)$, showing that the first prior has heavier tails and more mass concentrated at zero, while the second prior has more positive density on smaller, non-zero values. Compared to the priors in Figure 3b, which use the usual range of α with



(a) With $(k_1, k_2) = (0.5, 4)$.

(b) With the usual range $(k_1, k_2) = (1, 2)$.

Figure 3: Comparison of the GBR densities with $(e_1, f_1, e_2, f_2) = (0.1, 1, 2, 0.01)$ (dashed) and $(e_1, f_1, e_2, f_2) = (1, 1, 40, 0.5)$ (solid). Code for reproducing these plots is available at the GitHub repository for the R package `GMCB`.

$(k_1, k_2) = (1, 2)$, these priors have more mass concentrated at zero and small non-zero values and heavier tails, allowing better accommodation of sparse and dense settings. The results in Section 5 further suggest that the choice $(k_1, k_2) = (0.5, 2)$ yields better estimation in sparse settings, while $(k_1, k_2) = (0.5, 4)$ is more suitable for dense settings.

2.2 Tail-Robustness

The global-local structure of the GBR prior leads to the same sort of tail-robustness properties enjoyed by the horseshoe prior (Carvalho et al., 2010). Consider the following one-dimensional case of the model:

$$\begin{aligned}
 Y|\beta &\sim N(\beta, 1), \\
 \nu(\beta|\lambda, \alpha) &= \left(\frac{\alpha \lambda^{1/\alpha}}{2^{1/\alpha+1} \Gamma(1/\alpha)} \right) \exp \left\{ -\frac{\lambda}{2} |\beta|^\alpha \right\}, \\
 \lambda &\sim \frac{1}{2} \text{Gamma}(e_1, f_1) + \frac{1}{2} \text{Gamma}(e_2, f_2), \\
 \alpha &\sim \text{Unif}(k_1, k_2).
 \end{aligned}$$

Let $m(y)$ be the marginal density achieved by integrating over all the parameters. A standard calculation shows that the marginal posterior mean of β satisfies

$$\mathbb{E}(\beta|y) = y + \frac{d}{dy} \log m(y),$$

and hence the following result shows that the GBR prior satisfies a tail-robustness property, indicating that bias is small for large signals.

Theorem 1. There is some C_h which depends on the hyperparameters such that $|y -$

$\mathbb{E}(\beta|y)| \leq C_h$ and

$$\lim_{|y| \rightarrow \infty} \frac{d}{dy} \log m(y) = 0.$$

Proof. See Appendix A. □

In estimation and prediction, the GBR prior is competitive with popular methods such as the horseshoe (Carvalho et al., 2010) and the spike-and-slab lasso (Ročková and George, 2018). Simulation results and additional details, including sampling approaches, are available (Xiang, 2020).

3 The Generalized Mean-Covariance Bridge Prior

Consider now an extension of the GBR prior to mean and covariance estimation, where the response is modeled by the multivariate linear model in equation (1). Let $j:k$ denote the indices j through k , and let A^j denote column j of matrix A . As previously described, the modified Cholesky decomposition allows the model to be expressed as a sequence of autoregressions, with the j th autoregression's coefficients given by $-T_{j,1:(j-1)} = \delta_j^\top$ and its error variance given by $D_{jj} = \gamma_j$. Assuming ε_i is multivariate normal with mean zero and covariance matrix D , the likelihood of the Y_i , suppressing dependence on i , can be expressed as

$$\begin{aligned} Y_1 | X, B^1, \gamma_1 &\sim N((B^1)^\top X, \gamma_1), \\ Y_j | Y_{1:(j-1)}, X, B^{1:j}, \delta_j, \gamma_j &\sim N\left((B^j)^\top X + \sum_{k=1}^{j-1} \delta_{j,k} (Y_k - (B^k)^\top X), \gamma_j\right), \quad j = 2, \dots, q. \end{aligned} \tag{7}$$

Observe that B^j and δ_j are regression coefficients in a univariate-response linear regression, so the GBR prior in Section 2 can be directly specified on these parameters. However, there is little reason to expect the same penalty to be appropriate for B^j and δ_j , as the matrices B and T are not expected to have similar levels of sparsity. Thus the GBR prior is specified such that elements of B share a penalty parameter while elements of T share a separate penalty parameter. In particular, the prior on B^j is

$$\nu(B^j | \Lambda^j, \alpha_b, \gamma_j) \propto \exp\left\{-\frac{1}{2\gamma_j} \sum_{k=1}^p \lambda_{kj} |B_{kj}|^{\alpha_b}\right\}, \quad j = 1, \dots, q,$$

and the prior on δ_j is

$$\nu(\delta_j | \tau_j, \alpha_d, \gamma_j) \propto \exp\left\{-\frac{1}{2\gamma_j} \sum_{k=1}^{j-1} \tau_{j,k} |\delta_{j,k}|^{\alpha_d}\right\}, \quad j = 2, \dots, q.$$

For the remaining parameters, each of the regularization parameters λ_{kj} and $\tau_{j,k}$ follow two-component Gamma mixture priors, the penalty parameters α_b and α_d are independent and identically distributed (i.i.d.) $\text{Unif}(k_1, k_2)$, and the γ_j are i.i.d. $\text{IG}(a, b)$. The full hierarchical model is detailed in Appendix B, with the resulting posterior density characterized by equation (11).

The above prior is specified on (B, T, D) . The prior induced on (B, Ω) by this specification, marginalizing over the regularization parameters and the penalty parameters, is referred to as the generalized mean-covariance bridge (GMCB) prior. Similar to the GBR prior, when the regularization parameters and the penalty parameters are fixed, the posterior mode of B^j given δ_j is the frequentist bridge estimate, and vice versa.

4 Estimation and Sampling

For posterior inference on (B, Ω) under the GMCB prior, equation (3) is used to obtain posterior samples of Ω from samples of T and D . Point estimators are commonly selected to be the Bayes estimators under separate loss functions for B and Ω . A common choice of loss function is squared Frobenius loss for both B and Ω , resulting in the point estimator

$$(\hat{B}_F, \hat{\Omega}_F) = \left(\mathbb{E}(B|Y, X), \mathbb{E}(\Omega|Y, X) \right).$$

The following loss functions are also considered:

$$\begin{aligned} L_Q(\tilde{B}, B) &= \text{tr} \left((\tilde{B} - B)\Omega(\tilde{B} - B)^\top \right), \\ L_S(\tilde{\Omega}, \Omega) &= \text{tr}(\tilde{\Omega}\Omega^{-1}) - \log |\tilde{\Omega}\Omega^{-1}| - q. \end{aligned}$$

The loss function L_Q is the scalar quadratic loss (Yuasa and Kubokawa, 2021) and is based on the Kullback-Liebler (KL) divergence between two matrix normal distributions with the same precision matrix, and L_S is based on the KL divergence between two multivariate normal distributions with the same mean. The Bayes estimators under these loss functions (Yang and Berger, 1994; Yuasa and Kubokawa, 2021) are

$$(\hat{B}_Q, \hat{\Omega}_S) = \left(\mathbb{E}(B\Omega|Y, X) \left[\mathbb{E}(\Omega|Y, X) \right]^{-1}, \left[\mathbb{E}(\Omega^{-1}|Y, X) \right]^{-1} \right).$$

Closed-form expressions under the GMCB prior are not available for either of these point estimators, requiring Monte Carlo methods for estimation.

4.1 Markov Chain Monte Carlo

Two component-wise MCMC algorithms with invariant density characterized by equation (11) in Appendix B are developed. The full details of the posterior conditionals are provided in Appendix B.1. Among these, only the distributions for the λ_{kj} , $\tau_{j,k}$, and γ_j are standard distributions. The GMCB-MH algorithm is a component-wise sampling scheme that uses Gibbs updates for these parameters and random walk Metropolis-Hastings updates with Gaussian proposal distributions for the remaining parameters. All updates are univariate, as block updates for B^j and δ_j result in low acceptance rates, even for p and q small relative to n . For ease of notation, define γ to be the vector of γ_j 's, and δ and τ to be vectors of length $q(q-1)/2$ concatenating the δ_j and τ_j , respectively. The algorithm makes updates in the following order:

$$\begin{aligned} & (\Lambda, B, \alpha_b, \tau, \delta, \gamma, \alpha_d) \rightarrow (\Lambda', B, \alpha_b, \tau, \delta, \gamma, \alpha_d) \rightarrow (\Lambda', B', \alpha_b, \tau, \delta, \gamma, \alpha_d) \\ & \rightarrow (\Lambda', B', \alpha'_b, \tau, \delta, \gamma, \alpha_d) \rightarrow (\Lambda', B', \alpha'_b, \tau', \delta, \gamma, \alpha_d) \rightarrow (\Lambda', B', \alpha'_b, \tau', \delta', \gamma, \alpha_d) \\ & \rightarrow (\Lambda', B', \alpha'_b, \tau', \delta', \gamma', \alpha_d) \rightarrow (\Lambda', B', \alpha'_b, \tau', \delta', \gamma', \alpha'_d). \end{aligned}$$

This update order implies that initialization values for the regularization parameters Λ and τ are not required.

GMCB-MH is valid for all n , p , q , and $k_2 \geq 2$. However, a more computationally efficient algorithm is available when $k_2 = 2$. In this case, the exponential power distribution has a SMN representation (West, 1987). This property can be leveraged to replace the Metropolis-Hastings updates for B and δ in GMCB-MH with Gibbs updates. Although the SMN representation has been used for a data augmentation algorithm for the Bayesian bridge in multiple regression (Polson et al., 2014), the available implementation cannot be directly applied here because B and δ are not conditionally independent.

4.2 GMCB-SMN Algorithm

The GMCB-SMN algorithm updates B and δ by augmenting their posterior conditional distributions. The basic strategy for B is discussed here, with the full details and application of the strategy to sampling δ deferred to Appendix B.2. Both GMCB-SMN and GMCB-MH are implemented using the C++ interface provided in the Rcpp (Eddelbuettel et al., 2023a) and RcppAmaradillo (Eddelbuettel et al., 2023b) packages in the R package GMCB, which is freely available at <https://github.com/czhao15103/GMCB>.

Let p_a denote the density of a positive stable random variable with characteristic exponent $a < 1$. West (1987) showed that the mixing density in the SMN representation of the exponential power distribution is the density of a polynomially-tilted positive stable

random variable. Then the SMN representation of the prior on B_{kj} is given by

$$B_{kj}|\omega_{kj}, \lambda_{kj}, \gamma_j, \alpha_b \sim N\left(0, \frac{1}{\omega_{kj}} \left(\frac{2\gamma_j}{\lambda_{kj}}\right)^{2/\alpha_b}\right),$$

$$g(\omega_{kj}|\alpha_b) \propto \omega_{kj}^{-1/2} p_{\alpha_b/2}(\omega_{kj}), \quad \omega_{kj} > 0,$$

and the posterior conditional distribution of B can be obtained by marginalizing over the ω_{kj} :

$$q(B|Y, X, \Lambda, \alpha_b, \delta, \gamma, \tau, \alpha_d)$$

$$\propto \int_{\mathbb{R}_+^{pq}} \exp\left\{-\frac{1}{2} \text{tr}((Y - XB)\Omega(Y - XB)^\top)\right\}$$

$$\cdot \left[\prod_{k=1}^p \prod_{j=1}^q \nu(B_{kj}|\omega_{kj}, \lambda_{kj}, \gamma_j, \alpha_b) g(\omega_{kj}|\alpha_b) \right] d\omega. \quad (8)$$

The integrand of equation (8) will be referred to as the augmented posterior conditional distribution of B . To update B , the algorithm samples the conditional distributions associated with equation (8) for ω and then B and discards ω . Doing so will preserve the invariant density of the Markov chain and does not affect the other posterior conditional distributions.

The conditional distribution of ω_{kj} associated with equation (8) is the distribution of an exponentially-tilted positive stable random variable. Devroye (2009) proposed a double-rejection algorithm for sampling from this distribution that has been implemented in the R package `copula` (Hofert et al., 2020). A modified version of this implementation is used in the package `GMCB`.

For deriving the conditional distribution of B associated with equation (8), note that the contribution from the SMN representation of the exponential power prior is easily expressed as a multivariate normal distribution on $\text{vec}(B)$ with mean zero and a $pq \times pq$ diagonal covariance matrix Δ . Thus the derivation is straightforward when the likelihood can be expressed in terms of $\text{vec}(B)$. When $X^\top X$ is invertible, this can be accomplished by using the equivalence between a matrix normal distribution and a multivariate normal distribution. Routine calculation then shows that the conditional distribution under equation (8) is a multivariate normal. The expressions for the mean and covariance matrix can be found in Appendix B.2.

When $p \geq n$, the likelihood cannot be rewritten in this way, as it relies on the invertibility of $X^\top X$. However, a variable transformation for B using the SVD of X and the modified Cholesky decomposition of Ω makes it possible to sample with a multivariate normal distribution. Define $U \in \mathbb{R}^{n \times n}$ and $V \in \mathbb{R}^{p \times p}$ to be orthonormal matrices and $C \in \mathbb{R}^{n \times p}$ such that the SVD of X is given by $X = UCV^\top$. Define $\eta = V^\top B T^\top$. The

Jacobian of this transformation is a constant with respect to η , and letting \otimes denote the Kronecker product, the trace in the likelihood component can be rewritten in terms of η as

$$-2 \operatorname{vec}(C^\top U^\top Y T^\top D^{-1})^\top \operatorname{vec}(\eta) + \operatorname{vec}(\eta)^\top (D^{-1/2} \otimes C)^\top (D^{-1/2} \otimes C) \operatorname{vec}(\eta).$$

Although the matrix $(D^{-1/2} \otimes C)^\top (D^{-1/2} \otimes C)$ is not full rank, the contribution of the prior after transformation is

$$\exp \left\{ -\frac{1}{2} \operatorname{vec}(\eta)^\top (T^{-1} \otimes V)^\top \Delta (T^{-1} \otimes V) \operatorname{vec}(\eta) \right\}.$$

As T is unit lower triangular and V is orthonormal, $(T^{-1} \otimes V)^\top \Delta (T^{-1} \otimes V)$ is positive definite, so that the conditional distribution of $\operatorname{vec}(\eta)$ is multivariate normal.

In either case, updating B requires sampling from a pq -variate normal distribution. For sampling this distribution, the computational complexity of the approach in [Rue \(2001\)](#) is $O(p^3 q^3)$; that is, there exists a constant $M > 0$ such that the number of floating point operations required is bounded above by $M p^3 q^3$. Specific to GMCB-SMN, the computational complexity of the approach in [Bhattacharya et al. \(2016\)](#) is $O(np^2 q^3)$, as the matrix $(T^{-1} \otimes V)^\top \Delta (T^{-1} \otimes V)$ is not sparse. To sample as efficiently as possible, GMCB-SMN uses the approach in [Rue \(2001\)](#) when $p < n$ and the approach in [Bhattacharya et al. \(2016\)](#) when $p \geq n$. As shown in [Section 5.1](#), when $p \ll n$, this choice makes GMCB-SMN much faster than the HS-GHS algorithm, which always uses the approach in [Bhattacharya et al. \(2016\)](#) when updating B .

A similar augmentation strategy is used for the posterior conditional distribution of δ_j . The SMN representation expresses the prior on $\delta_{j,k}$ as

$$\begin{aligned} \delta_{j,k} | \epsilon_{j,k}, \tau_{j,k}, \gamma_j, \alpha_d &\sim N \left(0, \frac{1}{\epsilon_{j,k}} \left(\frac{2\gamma_j}{\tau_{j,k}} \right)^{2/\alpha_d} \right), \\ g(\epsilon_{j,k} | \alpha_d) &\propto \epsilon_{j,k}^{-1/2} p_{\alpha_d/2}(\epsilon_{j,k}), \quad \epsilon_{j,k} > 0. \end{aligned}$$

Like the ω_{kj} , the conditional distribution of each $\epsilon_{j,k}$ associated with the augmented posterior conditional distribution is an exponentially-tilted positive stable random variable. For the conditional distribution of δ_j associated with the augmented posterior conditional, standard calculations show that it is a $(j-1)$ -variate normal distribution for all values of n , p , and q . When updating δ_j , GMCB-SMN uses the approach in [Rue \(2001\)](#) when $j \leq n$ and the approach in [Bhattacharya et al. \(2016\)](#) when $j > n$.

4.2.1 Summarizing the GMCB-SMN Algorithm

By augmenting the posterior conditional distributions of B and δ , GMCB-SMN only requires Metropolis-Hastings updates for the penalty parameters α_b and α_d . Let ω and ϵ denote the collections of the latent scale variables for B and δ , respectively. The algorithm makes updates in the following order:

$$\begin{aligned}
& (B, \Lambda, \alpha_b, \delta, \tau, \gamma, \alpha_d) \rightarrow (\omega', B, \Lambda, \alpha_b, \delta, \tau, \gamma, \alpha_d) \\
\rightarrow & (\omega', B', \Lambda, \alpha_b, \delta, \tau, \gamma, \alpha_d) \rightarrow (\omega', B', \Lambda', \alpha_b, \delta, \tau, \gamma, \alpha_d) \\
\rightarrow & (\omega', B', \Lambda', \alpha'_b, \delta, \tau, \gamma, \alpha_d) \rightarrow (\omega', B', \Lambda', \alpha'_b, \epsilon', \delta, \tau, \gamma, \alpha_d) \\
\rightarrow & (\omega', B', \Lambda', \alpha'_b, \epsilon', \delta', \tau, \gamma, \alpha_d) \rightarrow (\omega', B', \Lambda', \alpha'_b, \epsilon', \delta', \tau', \gamma, \alpha_d) \\
\rightarrow & (\omega', B', \Lambda', \alpha'_b, \epsilon', \delta', \tau', \gamma', \alpha_d) \rightarrow (\omega', B', \Lambda', \alpha'_b, \epsilon', \delta', \tau', \gamma', \alpha'_d).
\end{aligned}$$

The latent scale variables ω' and ϵ' are discarded, and the posterior conditional distributions used to update Λ , α_b , τ , γ , and α_d are the same as those used in GMCB-MH.

4.3 Comparing GMCB-MH and GMCB-SMN

Although GMCB-SMN is not applicable for values $k_2 > 2$, it is much more efficient than GMCB-MH. For the scenarios described in Section 5, sampler efficiency was compared based on the computation time and the multivariate effective sample size (ESS) (Vats et al., 2019), which was computed using the R package `mcmcse` (Flegal et al., 2021), for $1e5$ iterations. As shown in Table 3 in Section 5, GMCB-MH has a much lower multivariate ESS. This is likely due to higher autocorrelation for B and δ , as illustrated in Figure 4. Autocorrelation for the remaining parameters tended to be similar between the two algorithms, which is expected as the sampling approach is the same for those parameters. While the difference in computation time shown in Figure 5 is not that large, changes in the relative size of p and q can have a significant impact. The scenarios in Section 5 have $p = q = 5$. For the data example described in Section 6, where $p = 1$ and $q = 253$, GMCB-MH required an average of 6-8 hours for 1000 iterations, while GMCB-SMN required only 20-30 minutes for 2000 iterations.

Remark 1. While it is possible to reduce the dimension of the posterior by integrating out Λ and τ , doing so does not result in any computational advantages – in fact, the elements of γ can no longer be sampled using standard distributions.

Remark 2. A data augmentation algorithm based on a scale mixture of uniforms (SMU) representation is also possible. The SMU representation has been used for the Bayesian bridge in multiple regression by Griffin and Hoff (2020) and Mallick and Yi (2018). Under this representation, truncated normal distributions are used to update B and δ . Although the algorithm is valid for $k_2 \geq 2$ and allows block Gibbs sampling of B , Gibbs sampling

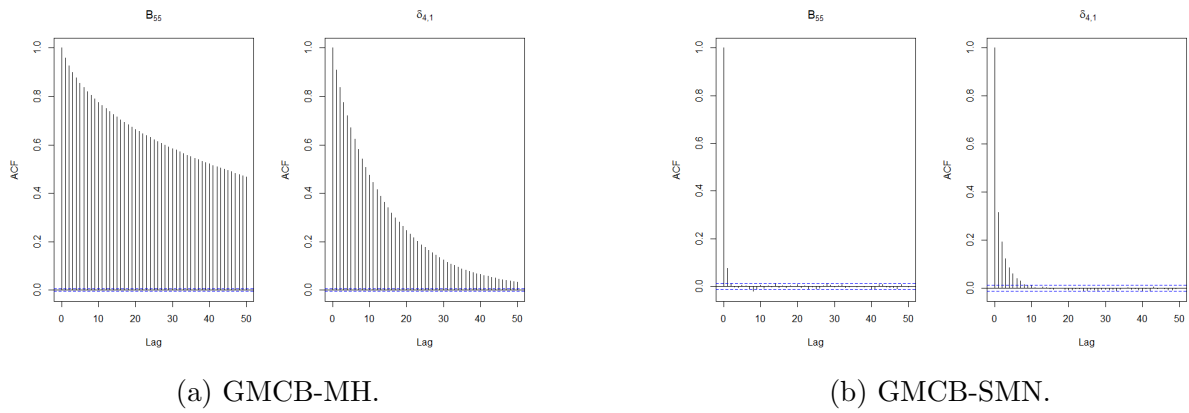


Figure 4: Autocorrelation plots for randomly selected elements of B and δ in Scenario 1 in Section 5. These plots are typical of what was observed in each scenario. Additional correlation plots for the other scenarios are available in the appendix.

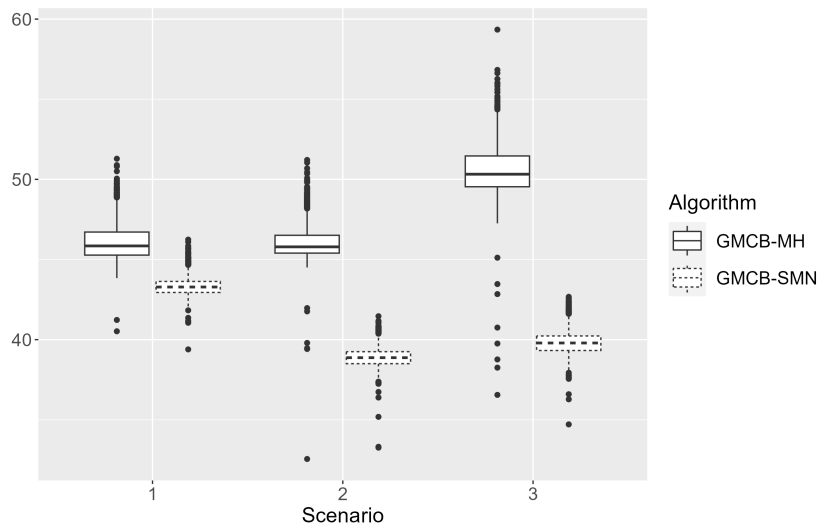


Figure 5: Comparison of GMCB-MH and GMCB-SMN based on total computation time in seconds for 100,000 iterations, based on 2000 replications.

of δ under the SMU representation requires $q \leq n$. This restriction can be addressed using a SVD-based transformation, but it would require $q - n$ SVDs to be computed at every iteration of the algorithm when $q > n$.

5 Simulations

Estimates for (B, Ω) from GMCB are compared with estimates from HS-GHS (Li et al., 2021) and mSSL (Deshpande et al., 2019). The following simulations compare the MAP estimates from both optimization algorithms for mSSL (DPE and DCPE) with the Bayes estimates $(\hat{B}_F, \hat{\Omega}_F)$ and $(\hat{B}_Q, \hat{\Omega}_S)$ from GMCB and HS-GHS. The MATLAB code by Li et al. (2021) was used for HS-GHS, and the R package mSSL (Deshpande, 2019) was used for mSSL. Code for replicating the simulations can be found at the GitHub repository for the R package GMCB.

In all simulations, $p = 5$, $q = 5$, and $n = 100$. For each scenario, the rows of X were drawn independently from $N_p(0, \Sigma_X)$, where the ij th element of Σ_X is $0.7^{|i-j|}$, and 2000 responses were generated from the model

$$Y = XB + E, \quad E \sim MVN_{n,p}(0, I_n, \Omega^{-1} = \Sigma).$$

Before estimation, the design matrix was standardized and the response matrix was centered. For hyperparameter settings, the default values in the package mSSL were used for mSSL-DPE and mSSL-DCPE. For both GMCB algorithms, $k_1 = 0.5$, while $k_2 = 2$ for GMCB-SMN and $k_2 = 4$ for GMCB-MH. An empirical prior specified using the method-of-moments was used for γ . The priors on the regularization parameters differed between scenarios. Extensive empirical work indicated that a Gamma(1, 1) and Gamma(40, 0.5) mixture prior works well in dense settings, while a Gamma(0.1, 1) and Gamma(2, 0.01) mixture prior is more suitable in sparse settings. The results presented use the first prior for both Λ and τ in Scenario 1 and the second prior for both in Scenario 2. In Scenario 3, the first prior was used for τ while the second was used for Λ .

The multivariate ESS approach (Vats et al., 2019) was used to determine the number of iterations for the GMCB-MH, GMCB-SMN, and HS-GHS samplers. The minimum ESS for the 40 parameters of interest as computed using the mcmcse package (Flegal et al., 2021) was 8438, and the number of iterations was selected so that the multivariate ESS was approximately twice the minimum ESS.

Scenario 1: The entries of the matrix B were independently drawn from $N(2, 0.001^2)$. The covariance matrix is compound symmetric with $\Sigma_{ij} = 0.7^{I\{i \neq j\}}$, so Ω is a dense

matrix. The parameters of the modified Cholesky decomposition are

$$\gamma = (1, 0.51, 0.424, 0.388, 0.368)^\top$$

and

$$\delta_{j,k} = \begin{cases} 0.7, & j = 2, \\ 0.412, & j = 3, \\ 0.292, & j = 4, \\ 0.226, & j = 5. \end{cases}$$

GMCB-MH, GMCB-SMN, and the HS-GHS algorithm were run for $1.5e5$, $2.5e4$, and $2.5e4$ iterations, respectively.

Scenario 2: The entries of the matrix B were independently drawn from $N(5, 1^2)$, and 12 entries were randomly set to zero. The covariance matrix has an AR(1) structure with $\Sigma_{ij} = 0.7^{|i-j|}$, so Ω is banded. The parameters of the modified Cholesky decomposition are

$$\gamma = (1, 0.51, 0.51, 0.51, 0.51)^\top$$

and

$$\delta_{j,k} = \begin{cases} 0.7, & k = j - 1, \\ 0, & \text{otherwise.} \end{cases}$$

GMCB-MH, GMCB-SMN, and the HS-GHS algorithm were run for $1.5e5$, $2.5e4$, and $2.5e4$ iterations, respectively.

Scenario 3: Three randomly selected coefficients in B were independently drawn from $N(15, 3^2)$, and the remaining coefficients were set to zero. The precision matrix was defined as in [Daniels and Pourahmadi \(2002\)](#) scenario IIIA:

$$\gamma = (0.5, 0.7, 1, 3, 5)^\top$$

and

$$\delta_{j,k} = \begin{cases} 0.75 + 0.02k, & k = j - 1, \\ 0.4, & k = j - 2, \\ 0.2, & k = j - 3, \\ 0.1, & k = j - 4. \end{cases}$$

This results in a nonstationary covariance matrix.

GMCB-MH, GMCB-SMN, and the HS-GHS algorithm were run for $1.5e5$, $2.75e4$, and $3e4$ iterations, respectively.

The average Frobenius loss for all scenarios is displayed in Table 2. (The results under L_S and L_Q , which show similar trends, are omitted). Estimation accuracy for B is similar across all scenarios for the three models. For estimation of Ω , the average loss for mSSL was nearly double that of the fully Bayesian approaches when Ω was dense (Scenarios 1 and 3). When Ω was sparse (Scenario 2), mSSL slightly outperformed the fully Bayesian approaches. The lack of local regularization parameters in mSSL may explain the difference in performance. mSSL uses the regularization parameter from the slab component of the spike-and-slab LASSO prior on the off-diagonal elements as the rate of the exponential prior on the diagonal elements of Ω . In both Scenarios 1 and 3, the diagonal elements of Ω are much larger in magnitude than the off-diagonal elements, while the magnitudes are similar in Scenario 2. Without local parameters, the same amount of regularization is applied to both the diagonal and non-zero off-diagonal elements.

Comparing the results for GMCB-MH and GMCB-SMN, the utility of allowing larger values for k_2 in dense scenarios is evident in the estimation of Ω . In Scenarios 1 and 3, the δ_j are dense with small signals, and extending the upper bound to $k_2 = 4$ places more prior mass on smaller, non-zero values, allowing GMCB-MH to outperform both GMCB-SMN and HS-GHS in both scenarios, while GMCB-SMN only outperforms HS-GHS in Scenario 3. When the δ_j are sparse (Scenario 2), extending the upper bound has little benefit, but both GMCB methods outperform HS-GHS. Increasing k_2 has little effect on estimation of B , even in Scenario 1, where B is dense.

5.1 Comparison of Computational Effort

The computational efficiency of the GMCB and HS-GHS algorithms were compared based on the computation time and multivariate ESS for $1e5$ iterations. The mSSL algorithms, which produce MAP estimates rather than posterior samples, are omitted from this comparison. For the scenarios in the previous section, the multivariate ESS of HS-GHS is comparable to that of GMCB-SMN in Scenario 1 but lower in the other two scenarios (Table 3), and the total computation time is much higher in all three scenarios (Table 4). HS-GHS always uses the approach of [Bhattacharya et al. \(2016\)](#) for sampling multivariate normals when updating B . Specific to HS-GHS, the computational complexity is $O(n^2pq^3)$, which is much higher compared to the $O(p^3q^3)$ complexity of the sampling approach in [Rue \(2001\)](#) used in GMCB-SMN, which does not depend on n .

However, when $p > n$, the linear scaling of computational complexity with p for HS-GHS makes it much faster than GMCB-SMN, which has computational complexity $O(np^2q^3)$ when using the method of [Bhattacharya et al. \(2016\)](#). Table 5 compares the

Table 2: Average squared Frobenius loss of \tilde{B} and $\tilde{\Omega}$ for GMCB, HS-GHS, and mSSL, based on 2000 replications. The maximum standard error for all values in the table was 0.060.

Scenario	$(\tilde{B}, \tilde{\Omega})$	Method	$\ \tilde{B} - B\ _F^2$	$\ \tilde{\Omega} - \Omega\ _F^2$
1	$(\hat{B}_F, \hat{\Omega}_F)$	GMCB-MH	0.944	2.454
		GMCB-SMN	0.944	3.612
		HS-GHS	0.920	3.471
	$(\hat{B}_Q, \hat{\Omega}_S)$	GMCB-MH	0.941	2.287
		GMCB-SMN	0.940	3.247
		HS-GHS	0.918	2.787
MAP	mSSL-DCPE	0.898	5.925	
	mSSL-DPE	0.899	5.972	
2	$(\hat{B}_F, \hat{\Omega}_F)$	GMCB-MH	1.286	1.706
		GMCB-SMN	1.227	1.265
		HS-GHS	1.437	1.862
	$(\hat{B}_Q, \hat{\Omega}_S)$	GMCB-MH	1.292	1.439
		GMCB-SMN	1.229	1.081
		HS-GHS	1.445	1.589
MAP	mSSL-DCPE	1.195	1.038	
	mSSL-DPE	1.194	1.045	
3	$(\hat{B}_F, \hat{\Omega}_F)$	GMCB-MH	3.331	0.741
		GMCB-SMN	3.293	0.827
		HS-GHS	3.338	0.934
	$(\hat{B}_Q, \hat{\Omega}_S)$	GMCB-MH	3.339	0.678
		GMCB-SMN	3.298	0.747
		HS-GHS	3.346	0.761
MAP	mSSL-DCPE	3.413	1.614	
	mSSL-DPE	3.402	1.524	

computation time for 500 iterations for $n = 100$, $p = 120$, and $q = 50$. Because 500 iterations are insufficient for effectively estimating over 7000 parameters, estimation results for this scenario are omitted. As expected, the required computation time is significantly higher for GMCB-SMN. Note that GMCB-MH is faster than both GMCB-SMN and HS-GHS for a fixed number of iterations, but achieving an acceptable multivariate ESS likely requires far more iterations for GMCB-MH.

6 The WISP Survey Example

The WFC3 Infrared Spectroscopic Parallel (WISP) Survey is a pure parallel Hubble Space Telescope (HST) program, meaning the data were collected by the Wide Field Camera

Table 3: Average multivariate ESS for GMCB-MH, GMCB-SMN, and HS-GHS for the scenarios in Section 5, based on 2000 replications. The maximum standard error for all values in the table was 1.916.

Scenario	$(\tilde{B}, \tilde{\Omega})$	GMCB-MH	GMCB-SMN	HS-GHS
1	$(\hat{B}_F, \hat{\Omega}_F)$	13470	77180	77400
	$(\hat{B}_Q, \hat{\Omega}_S)$	13250	81720	82400
2	$(\hat{B}_F, \hat{\Omega}_F)$	13572	83320	75670
	$(\hat{B}_Q, \hat{\Omega}_S)$	14070	83100	79300
3	$(\hat{B}_F, \hat{\Omega}_F)$	13760	72040	59800
	$(\hat{B}_Q, \hat{\Omega}_S)$	14070	71480	60400

Table 4: Average computation time in seconds for GMCB-MH, GMCB-SMN, and HS-GHS for the scenarios in Section 5, based on 2000 replications. The maximum standard error for all values in the table was 0.0677.

Scenario	GMCB-MH	GMCB-SMN	HS-GHS
1	46.11	43.33	1062
2	46.08	38.90	1060
3	50.55	39.80	1284

Table 5: Average computation time in hours for GMCB-MH, GMCB-SMN, and HS-GHS for a scenario with $n = 100$, $p = 120$, $q = 50$, based on 50 replications. The maximum standard error for all values in the table was 0.037.

GMCB-MH	GMCB-SMN	HS-GHS
2.6	46	6.3

3 (WFC3) while other HST instruments were in use. The survey used the WFC3’s two near-infrared grisms¹ (Atek et al., 2010), which cover different wavelengths – the G_{102} covers the 800-1150 nanometer (nm) range, while the G_{141} covers the 1075-1700 nm range (Dressel and Marinelli, 2023). By combining the spectra from the two grisms, it is possible to detect multiple emission lines for each object (Atek et al., 2010). The detection and identification of these lines are necessary for the scientific goals of the WISP survey, as they provide the distance of the galaxies and allow the measurement of galaxies’ physical properties (Dickinson et al., 2018). Visual inspection of these spectra would be time-consuming: the WISP survey has observed 483 fields² (Baronchelli et al., 2010), and each field includes hundreds, or even thousands, of spectra.

One-dimensional spectra (i.e., the flux, or brightness, at each observed wavelength) are extracted from the dispersed images and used for the detection of emission lines. In these

¹Grisms are combinations of a diffraction grating and a prism that can produce dispersed images of light spectra for all objects in the field of view (Weiner, 2012).

²Data is only available for 432 (Dickinson et al., 2018).

spectra, spurious features, e.g., due to contamination by stellar diffraction spikes, nearby continuum sources, or zeroth orders, may be mistaken for emission lines (Atek et al., 2010). However, visual inspection of the two-dimensional images and extracted spectra provides classifications for the emission lines as either genuine or spurious (Dickinson et al., 2018). In this analysis, the one-dimensional spectra are the input for GMCB. All analysis was conducted in R (R Core Team, 2022).

The data used for this analysis were restricted to fields that were covered by both gratings. Each spectrum is sampled into 254 wavelength bins. However, because each grating had a flux measurement for the wavelength 1149.5 nm, the two measurements were combined using a weighted average based on the measurement errors. Consequently, only $q = 253$ unique wavelengths were included in the analysis. About 16.6% of the considered spectra did not have measurement errors available and were removed. This filtering left 135,386 spectra from 258 fields.

Each spectrum was classified based on the presence or absence of emission lines as determined by a WISP emission-line catalog constructed by Bagley et al. (2020). For convenience, let C_0 denote the class of spectra with no emission lines and C_1 denote the class of spectra with emission lines. Any spectra not included in the catalog were placed in C_0 , which accounted for 129,529 of the available spectra. For spectra included in the catalog, the degree of reviewer agreement in the identification of the emission lines was used to filter spectra for C_1 . There were 3565 spectra with a high degree of reviewer agreement that were placed in C_1 , and the remaining 2292 spectra which were included in the catalog were placed in a separate class. Only spectra in C_0 and C_1 were used for this analysis. Due to class imbalance, the training and test samples were created using a stratified approach, with 70% of each class in the training sample and 30% in the test sample. This resulted in 90,670 spectra from C_0 and 2495 spectra from C_1 in the training sample.

The GMCB model was fitted to the training sample on the cuberoot scale. Even an assumption of marginal normality was unreasonable on the original scale of the data, so a variety of univariate transformations that preserved the sign of the flux measurements were considered, including the inverse hyperbolic sine and various root transformations. Among those considered, the cuberoot transformation resulted in the most improvement in terms of marginal normality for both classes, so the analysis proceeded on this scale. The results presented are based on $1e6$ iterations of GMCB-SMN and use the hyperparameters recommended for sparse settings in Section 2 with a $\text{Unif}(0.5, 2)$ prior on the penalty exponents and an empirical prior on γ elicited using the method of moments. Results of a sensitivity analysis are available in Appendix D and indicate minimal impact of the hyperparameters on estimation.

Figure 6 compares heatmaps of the log absolute value of the elements in the sample precision matrix, $\hat{\Omega}_F$, and $\hat{\Omega}_S$ for C_0 and C_1 . Visible in all six matrices is a light colored

pattern resembling a cross. These patterns occur at the wavelengths in the upper range of the G_{102} and the lower range of the G_{141} , where flux measurements are known to have more noise. The cross hatch appearance in the matrices for C_0 is likely due to the rearrangement of the wavelengths in preparing the spectra for analysis – the wavelengths in this region were out of order in the raw spectra. Although the cross hatch pattern is not visible in the matrices for C_1 , it is worth noting that there are 31,878 distinct elements being estimated from 2495 spectra.

There are two interesting band patterns in the GMCB-SMN estimates for C_0 . Only the narrower band is apparent in the sample precision matrix. This band spans the portion of the precision matrix corresponding to the wavelengths 835.1–1058.3 nm and 1261.1–1693.55 nm. The wider band that is only apparent in $\hat{\Omega}_F$ and $\hat{\Omega}_S$ spans the portion of the precision matrix that approximately corresponds to the wavelengths 871.1–1151.9 nm and 1154.15–1693.55 nm. Such patterns may be due to the presence of mislabeled spectra, which were not included in the catalog used for defining the classes. Larger partial covariances between flux measurements are expected between the wavelengths at which emission lines occur, because the presence of a particular gas will be indicated by the presence of all of its emission lines in the galaxy’s spectrum ([Spectroscopy 101, 2021](#)), though they may be difficult to detect. In addition, certain emission lines corresponding to different gases are often both detectable in the same spectrum ([Atek et al., 2010](#)), and larger partial covariances between the flux measurements at these wavelengths might also be expected. If this conjecture is correct, the plots of the wavelengths spanned by these bands should produce straight lines, because the ratio of the observed wavelengths for two different emission lines is a constant ([Imaging the Universe—The University of Iowa, 2023](#)). Figure 7 plots the longer wavelengths spanned by each band against the shorter wavelengths. Both plots show strong linear relationships, though the plot for the wider band exhibits some deviations from the predominant linear trend at the lower and upper ends. This suggests that the band patterns in the estimates may reflect the presence of emission lines at these wavelengths, though further investigation is required.

Remark 3. Estimates for the precision matrices from GMCB-MH, HS-GHS, and mSSL were not obtained. For this example, GMCB-MH requires 32,133 component-wise Metropolis-Hastings updates, and the time required to tune the proposal step sizes and obtain estimates was prohibitive. For HS-GHS, the algorithm could not be run on the training sample for C_0 . Updating the mean in this case, where $n = 90,670$ and $q = 253$, would require inversion of a 22,939,510 by 22,939,510 ($nq \times nq$) matrix on each iteration of the algorithm, which could not be completed with 128 GB of RAM. For mSSL, the available implementation was unable to fit the data without an artificial predictor.

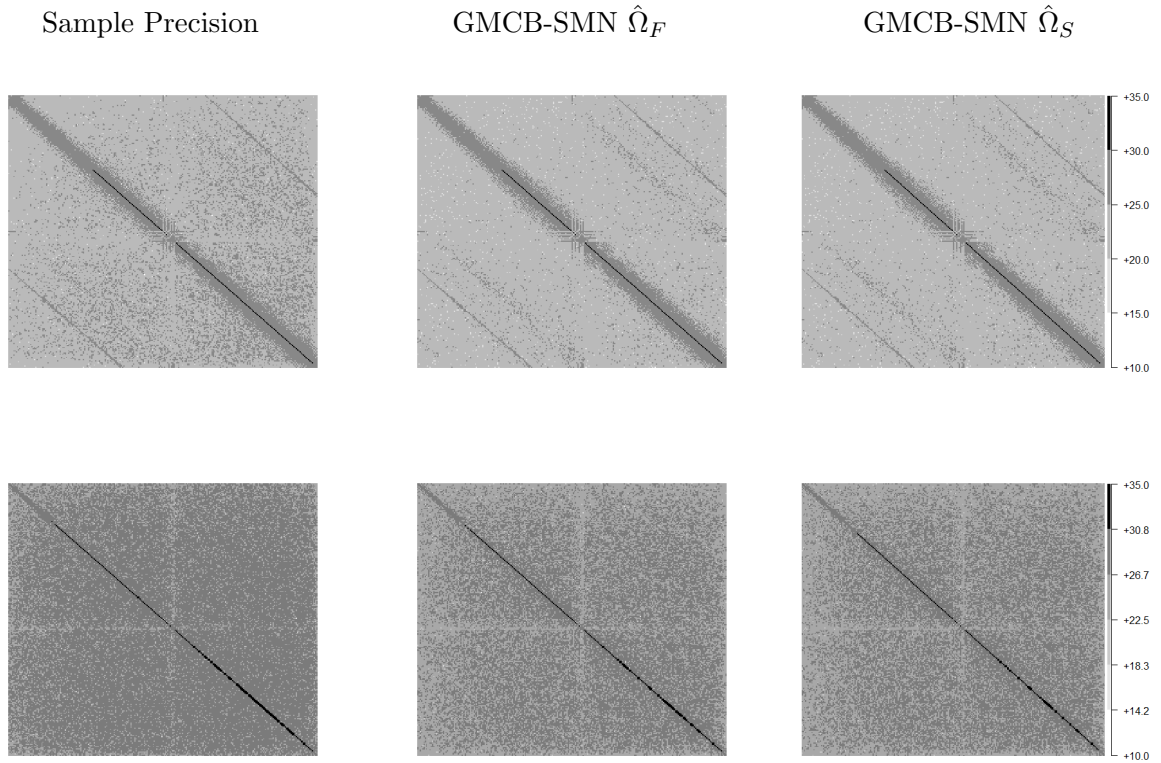
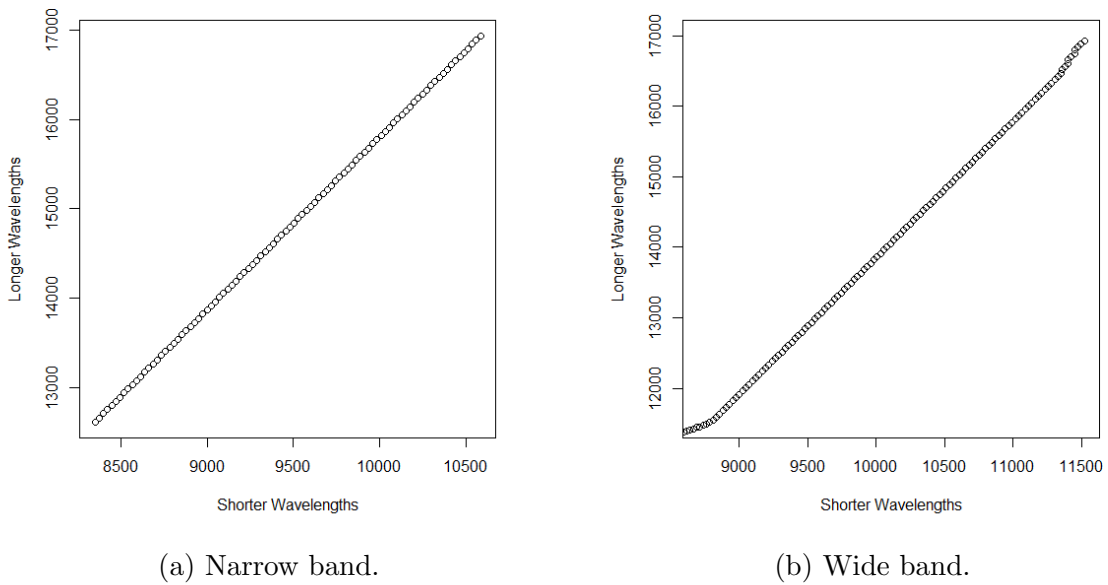


Figure 6: Log of the absolute value of entries of the estimated precision matrices, where darker colors correspond to larger values. The top row is for C_0 , and the bottom row is for C_1 .



(a) Narrow band.

(b) Wide band.

Figure 7: Plots of the wavelengths that correspond to the band structures visible in $\hat{\Omega}_F$ and $\hat{\Omega}_S$ for C_0 .

7 Final Remarks

Simultaneous mean and covariance estimation under a multivariate linear model was proposed using a novel penalized regression prior. The GBR prior allows the practitioner to address uncertainty in the regularization and penalty parameters in a principled manner by averaging over the posterior distribution. This is useful for simultaneous mean and covariance estimation, where there may be little prior information about the appropriate amount of penalization for the covariance or precision matrix. In the development of GMCB-SMN, selection of the sampling strategy for B based on the relative size of p and n enables the algorithm to handle data with large n , as demonstrated by the WISP survey example, and makes it much faster than the available HS-GHS algorithm for $p \ll n$.

There are a few extensions of this work that may be of particular interest for analyzing longitudinal data. It is common to measure covariates at each time point, so that the covariates associated with a single response vector Y_i may be a $q \times p$ matrix rather than a single vector of covariates. The mean regression coefficient B is then a p -length vector instead of a $p \times q$ matrix. The Gaussian likelihood can still be reparameterized into a sequence of autoregressions in this case, though efficient sampling of δ and B is likely to be more challenging than in the framework considered here.

Consider also the case where the covariance matrix of Y is known to be a sum of two positive definite matrices A and E . The regression framework used here can be extended to such cases by observing that if $Y \sim N_q(\mu, A + E)$, this distribution is the marginal distribution of Y in the hierarchy

$$\begin{aligned} Y|Z &\sim N_q(\mu, E), \\ Z &\sim N_q(0, A). \end{aligned}$$

The joint distribution of Y and Z is the product of two normal distributions, each of which can be rewritten in the regression framework of the modified Cholesky decomposition. Thus both A and E can be estimated using a prior such as the GMCB prior. This hierarchy can be generalized to fit linear mixed models, as well as error-in-variable linear regression models.

Acknowledgement

The authors thank Claudia Scarlata and Hugh Dickinson for providing the WISP survey data. The authors would also like to thank Claudia Scarlata for helpful discussions on the WISP survey analysis.

References

- Armagan, A. (2009). Variational bridge regression. In *Artificial Intelligence and Statistics*, pages 17–24. PMLR.
- Atek, H., Malkan, M., McCarthy, P., Teplitz, H. I., Scarlata, C., Siana, B., Henry, A., Colbert, J. W., Ross, N. R., Bridge, C., Bunker, A. J., Dressler, A., Fosbury, R. A. E., Martin, C., and Shim, H. (2010). The WFC3 Infrared Spectroscopic Parallel (WISP) Survey. *The Astrophysical Journal*, 723:104–115.
- Bagley, M. B., Scarlata, C., Mehta, V., Teplitz, H., Baronchelli, I., Eisenstein, D. J., Pozzetti, L., Cimatti, A., Rutkowski, M., Wang, Y., and Merson, A. (2020). HST grism-derived forecasts for future galaxy redshift surveys. *The Astrophysical Journal*, 897(98).
- Baronchelli, I., Scarlata, C. M., Rodighiero, G., noz, L. R.-M., Bonato, M., Bagley, M., Henry, A., Rafelski, M., Malkan, M., Colbert, J., Dai, Y. S., Dickinson, H., Mancini, C., Mehta, V., Morselli, L., and Teplitz, H. I. (2010). Identification of single spectral lines through supervised machine learning in a large HST survey (WISP): A pilot study for Euclid and WFIRST. *The Astrophysical Journal Supplement Series*, 249(12).
- Bhadra, A. and Mallick, B. K. (2013). Joint high-dimensional Bayesian variable and covariance selection with an application to eQTL analysis. *Biometrics*, 69:447–457.
- Bhattacharya, A., Chakraborty, A., and Mallick, B. K. (2016). Fast sampling with Gaussian scale mixture priors in high-dimensional regression. *Biometrika*, 103(4):985–991.
- Bottolo, L., Banterle, M., Richardson, S., Ala-Korpela, M., Järvelin, M.-R., and Lewin, A. (2021). A computationally efficient Bayesian seemingly unrelated regressions model for high-dimensional quantitative trait loci discovery. *Journal of the Royal Statistical Society, Series C*, 70:886–908.
- Cai, T. T., Li, H., Liu, W., and Xie, J. (2013). Covariate-adjusted precision matrix estimation with an application in genetical genomics. *Biometrika*, 100(1):139–156.
- Carvalho, C. M., Polson, N. G., and Scott, J. G. (2010). The horseshoe estimator for sparse signals. *Biometrika*, 97(2):465–480.
- Daniels, M. J. and Pourahmadi, M. (2002). Bayesian analysis of covariance matrices and dynamic models for longitudinal data. *Biometrika*, 89(3):553–566.
- Deshpande, S. K. (2019). *mSSL: The Multivariate Spike-and-Slab LASSO*. R package version 1.0.

- Deshpande, S. K., Ročková, V., and George, E. I. (2019). Simultaneous variable and covariance selection with the multivariate spike-and-slab LASSO. *Journal of Computational and Graphical Statistics*, 28(4):921–931.
- Devroye, L. (2009). Random variate generation for exponentially and polynomially tilted stable distributions. *ACM Transactions on Modeling and Computer Simulation*, 19(4):1–20.
- Dickinson, H., Scarlata, C., Fortson, L., Bagley, M., Mehta, V., Phillips, J., Baronchelli, I., Dai, S., Hathi, N., Henry, A., Malkan, M., Rafelski, M., Teplitz, H., Zanella, A., and Lintott, C. (2018). Galaxy Nurseries: Crowdsourced analysis of slitless spectroscopic data.
- Dressel, L. and Marinelli, M. (2023). Wide Field Camera 3 Instrument Handbook, version 15.0. Baltimore: STScI.
- Eddelbuettel, D., Francois, R., Allaire, J., Ushey, K., Kou, Q., Russell, N., Ucar, I., Bates, D., and Chambers, J. (2023a). *Rcpp: Seamless R and C++ Integration*. R package version 1.0.11.
- Eddelbuettel, D., Francois, R., Bates, D., Ni, B., and Sanderson, C. (2023b). *RcppArmadillo: 'Rcpp' Integration for the 'Armadillo' Templated Linear Algebra Library*. R package version 0.12.0.1.0.
- Flegal, J. M., Hughes, J., Vats, D., Dai, N., Gupta, K., and Maji, U. (2021). *mcmcse: Monte Carlo Standard Errors for MCMC*. Riverside, CA, and Kanpur, India. R package version 1.5-0.
- Frank, I. E. and Friedman, J. H. (1993). A statistical view of some chemometrics regression tools. *Technometrics*, 35(2):109–135.
- Fu, W. J. (1998). Penalized regressions: The bridge versus the Lasso. *Journal of Computational and Graphical Statistics*, 7(3):397–416.
- Gramacy, R. B. and Pantaleo, E. (2010). Shrinkage regression for multivariate inference with missing data, and an application to portfolio balancing. *Bayesian Analysis*, 5(2):237–262.
- Griffin, M. and Hoff, P. D. (2020). Testing sparsity-inducing penalties. *Journal of Computational and Graphical Statistics*, 29(1):128–139.
- Hoerl, A. E. and Kennard, R. W. (1970). Ridge regression: Biased estimation for nonorthogonal problems. *Technometrics*, 12(1):55–67.

- Hofert, M., Kojadinovic, I., Maechler, M., and Yan, J. (2020). *copula: Multivariate Dependence with Copulas*. R package version 1.0-1.
- Huang, J. Z., Liu, N., Pourahmadi, M., and Liu, L. (2006). Covariance matrix selection and estimation via penalised normal likelihood. *Biometrika*, 93(1):85–98.
- Imaging the Universe—The University of Iowa (2023). Astronomical Redshift. Retrieved November 20, 2023.
- Jalali, P., Khare, K., and Michailidis, G. (2020). B-CONCORD—a scalable Bayesian high-dimensional precision matrix estimation procedure.
- Kang, X. and Deng, X. (2020). An improved modified Cholesky decomposition approach for precision matrix estimation. *Journal of Statistical Computation and Simulation*.
- Kidd, B. and Katzfuss, M. (2022). Bayesian nonstationary and nonparametric covariance estimation for large spatial data. *Bayesian Analysis*, 17(1):291–351.
- Lee, K. and Lee, J. (2021). Estimating large precision matrices via modified Cholesky decomposition. *Statistica Sinica*, 31:173–196.
- Lee, K., Lee, J., and Lin, L. (2019). Minimax posterior convergence rates and model selection consistency in high-dimensional DAG models based on sparse Cholesky factors. *The Annals of Statistics*, 47(6):3413–3437.
- Lee, K. and Lin, L. (2023). Scalable Bayesian high-dimensional local dependence learning. *Bayesian Analysis*, 18(1):25–47.
- Lee, W. and Liu, Y. (2012). Simultaneous multiple response regression and inverse covariance matrix estimation via penalized Gaussian maximum likelihood. *Journal of Multivariate Analysis*, 111:241–255.
- Levina, E., Rothman, A., and Zhu, J. (2008). Sparse estimation of large covariance matrices via a nested Lasso penalty. *The Annals of Applied Statistics*, 2(1):245–263.
- Li, Y., Datta, J., Craig, B. A., and Bhadra, A. (2021). Joint mean-covariance estimation via the horseshoe. *Journal of Multivariate Analysis*, 183:104716.
- Mallick, H. and Yi, N. (2018). Bayesian bridge regression. *Journal of Applied Statistics*, 45(6):988–1008.
- Meinhausen, N. and Bühlmann, P. (2006). High-dimensional graphs and variable selection with the lasso. *The Annals of Statistics*, 34(3):1436–1462.
- Park, T. and Casella, G. (2008). The Bayesian Lasso. *Journal of the American Statistical Association*, 103(482):681–686.

- Polson, N. G., Scott, J. G., and Windle, J. (2014). The Bayesian bridge. *Journal of the Royal Statistical Society, Series B: Statistical Methodology*, 76:713–733.
- Pourahmadi, M. (1999). Joint mean-covariance models with applications to longitudinal data: Unconstrained parameterisation. *Biometrika*, 86(3):677–690.
- R Core Team (2022). *R: A Language and Environment for Statistical Computing*. R Foundation for Statistical Computing, Vienna, Austria.
- Ročková, V. and George, E. I. (2018). The spike-and-slab LASSO. *Journal of the American Statistical Association*, 113(521):431–444.
- Rothman, A. J., Levina, E., and Zhu, J. (2010). Sparse multivariate regression with covariance estimation. *Journal of Computational and Graphical Statistics*, 19(4):947–962.
- Rue, H. (2001). Fast sampling of Gaussian Markov random fields. *Journal of the Royal Statistical Society, Series B*, 63(2):325–338.
- Samanta, S., Khare, K., and Michailidis, G. (2022). A generalized likelihood-based Bayesian approach for scalable joint regression and covariance selection in high dimensions. *Statistics and Computing*, 32(47).
- Smith, M. and Kohn, R. (2002). Parsimonious covariance matrix estimation for longitudinal data. *Journal of the American Statistical Association*, 97(460):1141–1153.
- Spectroscopy 101 (2021). Beyond Temperature and Composition. Retrieved November 27, 2023.
- Tibshirani, R. (1996). Regression shrinkage and selection via the Lasso. *Journal of the Royal Statistical Society, Series B*, 58(1):267–288.
- Vats, D., Flegal, J. M., and Jones, G. L. (2019). Multivariate output analysis for Markov chain Monte Carlo. *Biometrika*, 106(2):321–337.
- Weiner, B. (2012). CANDELS Spectroscopy: The Infrared Grism.
- West, M. (1987). On scale mixtures of normal distributions. *Biometrika*, 74(3):646–648.
- Williams, D. R., Piironen, J., Vehtari, A., and Rast, P. (2018). Bayesian estimation of Gaussian graphical models with predictive covariance selection.
- Wu, W. B. and Pourahmadi, M. (2003). Nonparametric estimation of large covariance matrices of longitudinal data. *Biometrika*, 90:831–844.
- Xiang, D. (2020). Fully Bayesian penalized regression with a generalized bridge prior.

Yang, R. and Berger, J. O. (1994). Estimation of a covariance matrix using the reference prior. *The Annals of Statistics*, 22(3):1195–1211.

Yuan, M. and Lin, Y. (2007). Model selection and estimation in the Gaussian graphical model. *Biometrika*, 94(1):19–35.

Yuasa, R. and Kubokawa, T. (2021). Generalized Bayes estimators with closed forms for the normal mean and covariance matrices.

Zheng, H., Tsui, K.-W., Kang, X., and Deng, X. (2017). Cholesky-based model averaging for covariance matrix estimation. *Statistical Theory and Related Fields*, 1(1):48–58.

Appendices

A Proof of Theorem 1

Proof. Notice that

$$m(y) = \frac{1}{k_2 - k_1} \int \int \frac{1}{\sqrt{2\pi}} \exp\left(-\frac{(\beta - y)^2}{2}\right) \frac{\alpha}{2^{1/\alpha+1}\Gamma(1/\alpha)} \cdot \left\{ \frac{1}{2} \frac{f_1^{e_1}}{\Gamma(e_1)} \frac{\Gamma(e_1 + 1/\alpha)}{(|\beta|^\alpha/2 + f_1)^{e_1+1/\alpha}} + \frac{1}{2} \frac{f_2^{e_2}}{\Gamma(e_2)} \frac{\Gamma(e_2 + 1/\alpha)}{(|\beta|^\alpha/2 + f_2)^{e_2+1/\alpha}} \right\} d\beta d\alpha.$$

For ease of computation assume that $e_1 = e_2 = e$, $f_1 = f_2 = f$ and therefore

$$m(y) = \frac{1}{k_2 - k_1} \int \int \frac{1}{\sqrt{2\pi}} \exp\left(-\frac{(\beta - y)^2}{2}\right) \frac{\alpha}{2^{1/\alpha+1}\Gamma(1/\alpha)} \cdot \frac{f^e}{\Gamma(e)} \frac{\Gamma(e + 1/\alpha)}{(|\beta|^\alpha/2 + f)^{e+1/\alpha}} d\beta d\alpha$$

and

$$m'(y) = \frac{1}{k_2 - k_1} \int \int \frac{1}{\sqrt{2\pi}} (\beta - y) \exp\left(-\frac{(\beta - y)^2}{2}\right) \frac{\alpha}{2^{1/\alpha+1}\Gamma(1/\alpha)} \cdot \frac{f^e}{\Gamma(e)} \frac{\Gamma(e + 1/\alpha)}{(|\beta|^\alpha/2 + f)^{e+1/\alpha}} d\beta d\alpha.$$

Set

$$g(y) = \int \exp\left(-\frac{(\beta - y)^2}{2}\right) \frac{1}{(|\beta|^\alpha/2 + f)^{e+1/\alpha}} d\beta$$

$$h(y) = \int (\beta - y) \exp\left(-\frac{(\beta - y)^2}{2}\right) \frac{1}{(|\beta|^\alpha/2 + f)^{e+1/\alpha}} d\beta.$$

Let $t = \beta - y$ so that

$$g(y) = \int \exp\left(-\frac{t^2}{2}\right) \frac{1}{(|t + y|^\alpha/2 + f)^{e+1/\alpha}} dt$$

$$h(y) = \int t \exp\left(-\frac{t^2}{2}\right) \frac{1}{(|t + y|^\alpha/2 + f)^{e+1/\alpha}} dt$$

while if $t = -t$ then

$$g(y) = \int \exp\left(-\frac{t^2}{2}\right) \frac{1}{(|y - t|^\alpha/2 + f)^{e+1/\alpha}} dt$$

$$h(y) = - \int t \exp\left(-\frac{t^2}{2}\right) \frac{1}{(|y - t|^\alpha/2 + f)^{e+1/\alpha}} dt.$$

Hence

$$2g(y) = \int \exp\left(-\frac{t^2}{2}\right) \left[(|y + t|^\alpha/2 + f)^{-e-1/\alpha} + (|t - y|^\alpha/2 + f)^{-e-1/\alpha} \right] dt$$

$$2h(y) = \int t \exp\left(-\frac{t^2}{2}\right) \left[(|y + t|^\alpha/2 + f)^{-e-1/\alpha} - (|t - y|^\alpha/2 + f)^{-e-1/\alpha} \right] dt.$$

Notice that both functions under the integral sign are even. Thus

$$g(y) = \int_0^\infty \exp\left(-\frac{t^2}{2}\right) \left[(|y + t|^\alpha/2 + f)^{-e-1/\alpha} + (|t - y|^\alpha/2 + f)^{-e-1/\alpha} \right] dt$$

$$h(y) = \int_0^\infty t \exp\left(-\frac{t^2}{2}\right) \left[(|y + t|^\alpha/2 + f)^{-e-1/\alpha} - (|t - y|^\alpha/2 + f)^{-e-1/\alpha} \right] dt.$$

Suppose $y > 0$ (a nearly identical proof will hold with $y < 0$). Then

$$\begin{aligned} g(y) &> \int_0^\infty \exp\left(-\frac{t^2}{2}\right) (|t - y|^\alpha/2 + f)^{-e-1/\alpha} dt \\ &> \int_0^{y/2} \exp\left(-\frac{t^2}{2}\right) (|t - y|^\alpha/2 + f)^{-e-1/\alpha} dt \\ &= \int_0^{y/2} \exp\left(-\frac{t^2}{2}\right) ((y - t)^\alpha/2 + f)^{-e-1/\alpha} dt \\ &> \int_0^{y/2} \exp\left(-\frac{t^2}{2}\right) (y^\alpha/2 + f)^{-e-1/\alpha} dt \\ &= C_1 \cdot (y^\alpha/2 + f)^{-e-1/\alpha}, \end{aligned} \tag{9}$$

where $C_1 < \frac{\sqrt{2\pi}}{2}$. Next consider

$$\begin{aligned} -h(y) &= \int_0^\infty t \exp\left(-\frac{t^2}{2}\right) \left[(|t - y|^\alpha/2 + f)^{-e-1/\alpha} - (|y + t|^\alpha/2 + f)^{-e-1/\alpha} \right] dt \\ &= h_1(y) + h_2(y), \end{aligned}$$

where

$$h_1(y) = \int_0^{y/2} t \exp\left(-\frac{t^2}{2}\right) \left[((y-t)^\alpha/2 + f)^{-e-1/\alpha} - ((y+t)^\alpha/2 + f)^{-e-1/\alpha} \right] dt$$

$$h_2(y) = \int_{y/2}^\infty t \exp\left(-\frac{t^2}{2}\right) \left[(|t-y|^\alpha/2 + f)^{-e-1/\alpha} - (|y+t|^\alpha/2 + f)^{-e-1/\alpha} \right] dt.$$

Set

$$S(t) = ((y-t)^\alpha/2 + f)^{-e-1/\alpha} - ((y+t)^\alpha/2 + f)^{-e-1/\alpha}.$$

The next step is to show that, when $0 < t < y/2$,

$$S(t) < V(t) = 4\alpha(e+1/\alpha)((y/2)^\alpha/2 + f)^{-e-1/\alpha} \frac{t}{y}.$$

First notice that $S(0) = V(0) = 0$ so that it suffices to show that $S'(t) < V'(t)$. Consider

$$S'(t) = \frac{\alpha(e+1/\alpha)}{2} (y-t)^{\alpha-1} \left(\frac{(y-t)^\alpha}{2} + f \right)^{-(e+1/\alpha+1)}$$

$$+ \frac{\alpha(e+1/\alpha)}{2} (y+t)^{\alpha-1} \left(\frac{(y+t)^\alpha}{2} + f \right)^{-(e+1/\alpha+1)}$$

$$V'(t) = ((y/2)^\alpha/2 + f)^{-e-1/\alpha} \cdot \frac{1}{y} \cdot 4\alpha(e+1/\alpha).$$

Notice that

$$f(x) = x^{\alpha-1} \left(\frac{x^\alpha}{2} + f \right)^{-(e+1/\alpha+1)} = x^{-(2+\alpha e)} \left(\frac{1}{2} + \frac{f}{x^\alpha} \right)^{-(e+1+1/\alpha)}$$

is a decreasing function when x is large and $0 < k_1 < \alpha < k_2 \leq 4$. Thus, when y is large and $0 < t < y/2$, $y-t > y/2$ and $y+t > y > y/2$. Therefore,

$$yS'(t) = \frac{\alpha(e+1/\alpha)}{2} y(y-t)^{\alpha-1} \left(\frac{(y-t)^\alpha}{2} + f \right)^{-(e+1/\alpha+1)}$$

$$+ \frac{\alpha(e+1/\alpha)}{2} y(y+t)^{\alpha-1} \left(\frac{(y+t)^\alpha}{2} + f \right)^{-(e+1/\alpha+1)}$$

$$< \alpha(e+1/\alpha) y (y/2)^{\alpha-1} \left(\frac{(y/2)^\alpha}{2} + f \right)^{-(e+1/\alpha+1)}$$

$$< \alpha(e+1/\alpha) y (y/2)^{\alpha-1} \left(\frac{(y/2)^\alpha}{2} \right)^{-1} \left(\frac{(y/2)^\alpha}{2} + f \right)^{-(e+1/\alpha)}$$

$$= 4\alpha(e+1/\alpha) ((y/2)^\alpha/2 + f)^{-e-1/\alpha},$$

which gives $S'(t) < V'(t)$. So $S(t) < V(t)$. Then

$$\begin{aligned}
h_1(y) &= \int_0^{y/2} t \exp\left(-\frac{t^2}{2}\right) S(t) dt \\
&< \int_0^{y/2} t^2 \exp\left(-\frac{t^2}{2}\right) ((y/2)^\alpha/2 + f)^{-e-1/\alpha} \cdot \frac{1}{y} \cdot 4\alpha(e+1/\alpha) dt \\
&< ((y/2)^\alpha/2 + f)^{-e-1/\alpha} \cdot \frac{1}{y} \cdot 4\alpha(e+1/\alpha) \int_{-\infty}^{\infty} t^2 \exp\left(-\frac{t^2}{2}\right) dt \\
&< ((y/2)^\alpha/2 + f)^{-e-1/\alpha} \cdot \frac{1}{y} \cdot 4\alpha(e+1/\alpha) \cdot 2\sqrt{2\pi}
\end{aligned}$$

and

$$\begin{aligned}
h_2(y) &= \int_{y/2}^{\infty} t \exp\left(-\frac{t^2}{2}\right) \left[(|t-y|^\alpha/2 + f)^{-e-1/\alpha} - (|y+t|^\alpha/2 + f)^{-e-1/\alpha} \right] dt \\
&< \int_{y/2}^{\infty} t \exp\left(-\frac{t^2}{2}\right) (|t-y|^\alpha/2 + f)^{-e-1/\alpha} dt \\
&< f^{-e-1/\alpha} \int_{y/2}^{\infty} t \exp\left(-\frac{t^2}{2}\right) dt \\
&= f^{-e-1/\alpha} \exp\left(-\frac{y^2}{8}\right).
\end{aligned}$$

Therefore,

$$\begin{aligned}
-h(y) &= h_1(y) + h_2(y) \\
&< ((y/2)^\alpha/2 + f)^{-e-1/\alpha} \cdot \frac{1}{y} \cdot 4\alpha(e+1/\alpha) \cdot 2\sqrt{2\pi} + f^{-e-1/\alpha} \exp\left(-\frac{y^2}{8}\right). \quad (10)
\end{aligned}$$

By equations (9) and (10),

$$\begin{aligned}
0 < -\frac{m'(y)}{m(y)} &= \frac{\int -h(y) \frac{\alpha\Gamma(e+1/\alpha)}{2^{1/\alpha}\Gamma(1/\alpha)} d\alpha}{\int g(y) \frac{\alpha\Gamma(e+1/\alpha)}{2^{1/\alpha}\Gamma(1/\alpha)} d\alpha} \\
&< \frac{1}{y} \frac{\int \frac{\alpha\Gamma(e+1/\alpha)}{2^{1/\alpha+1}\Gamma(1/\alpha)} \left[((y/2)^\alpha/2 + f)^{-e-1/\alpha} 8\alpha(e+1/\alpha) \right] d\alpha}{\int \frac{\alpha\Gamma(e+1/\alpha)}{2^{1/\alpha+1}\Gamma(1/\alpha)} C_1(y^\alpha/2 + f)^{-e-1/\alpha} (2\pi)^{-1/2} d\alpha} \\
&\quad + \frac{\int \frac{\alpha\Gamma(e+1/\alpha)}{2^{1/\alpha+1}\Gamma(1/\alpha)} \left[f^{-e-1/\alpha} (2\pi)^{-1/2} \exp\left(-\frac{y^2}{8}\right) \right] d\alpha}{\int \frac{\alpha\Gamma(e+1/\alpha)}{2^{1/\alpha+1}\Gamma(1/\alpha)} C_1(y^\alpha/2 + f)^{-e-1/\alpha} (2\pi)^{-1/2} d\alpha} \\
&\equiv \frac{1}{y} A_1 + A_2.
\end{aligned}$$

Notice that A_1 is bounded by a constant since

$$\begin{aligned}
A_1 &= \frac{\int \frac{\alpha\Gamma(e+1/\alpha)}{2^{1/\alpha+1}\Gamma(1/\alpha)} \left[((y/2)^\alpha/2 + f)^{-e-1/\alpha} 8\alpha(e+1/\alpha) \right] d\alpha}{\int \frac{\alpha\Gamma(e+1/\alpha)}{2^{1/\alpha+1}\Gamma(1/\alpha)} C_1(y^\alpha/2 + f)^{-e-1/\alpha} (2\pi)^{-1/2} d\alpha} \\
&\leq \frac{\int \frac{k_2\Gamma(e+1/k_1)}{2^{1/k_2+1}\Gamma(1/k_2)} \left[((y/2)^\alpha/2 + f)^{-e-1/\alpha} 8k_2(e+1/k_1) \right] d\alpha}{\int \frac{k_1\Gamma(e+1/k_2)}{2^{1/k_1+1}\Gamma(1/k_1)} C_1(y^\alpha/2 + f)^{-e-1/\alpha} (2\pi)^{-1/2} d\alpha} \\
&\equiv C_{e,f,k_1,k_2}^{(0)} \frac{\int ((y/2)^\alpha/2 + f)^{-e-1/\alpha} d\alpha}{\int (y^\alpha/2 + f)^{-e-1/\alpha} d\alpha} \\
&< C_{e,f,k_1,k_2}^{(0)} \frac{\int (y^\alpha/2 + f)^{-e-1/\alpha} d\alpha}{\int (y^\alpha/2 + f)^{-e-1/\alpha} d\alpha} = C_{e,f,k_1,k_2}^{(0)}.
\end{aligned}$$

Notice that, because of the term $\exp\{-y^2/8\}$, A_2 is a higher order term of A_1 when y goes to infinity. Then

$$\frac{1}{y} A_1 + A_2 = \frac{1}{y} C_{e,f,k_1,k_2}^{(1)} + o\left(\frac{1}{y}\right) C_{e,f,k_1,k_2}^{(2)} \sim O(1/y)$$

since $C_{e,f,k_1,k_2}^{(1)} < C_{e,f,k_1,k_2}^{(0)}$ and $C_{e,f,k_1,k_2}^{(2)}$ are constants depending on the choice of k_1, k_2, e, f . Therefore $\lim_{y \rightarrow \infty} m'(y)/m(y) = 0$. \square

B Sampling Algorithms for GMCB

Recall that $j:k$ denotes the indices j through k and that A^j denotes column j of matrix A . In the following, $\text{IG}(a, b)$ and $\text{Gamma}(a, b)$ denote the shape-rate parameterization of the inverse Gamma and Gamma distributions, respectively.

The fully specified model under the GMCB prior is as follows. The likelihood is given by

$$Y_i|X_i, B, \Omega^{-1} \sim N_q(B^\top X_i, \Omega^{-1}), \quad i = 1, \dots, n.$$

Under the modified Cholesky decomposition, this is equivalent to

$$\begin{aligned} Y^1|X, B^1, \gamma_1 &\sim N_n(XB^1, \gamma_1 I_n), \\ Y^j|Y^{1:(j-1)}, X, B^{1:j}, \delta_j, \gamma_j &\sim N_n(XB^j + (Y^{1:(j-1)} - XB^{1:(j-1)})\delta_j, \gamma_j I_n), \quad j = 2, \dots, q. \end{aligned}$$

The prior on B^j for $j = 1, \dots, q$ is given by

$$\begin{aligned} \nu(B^j|\Lambda^j, \alpha_b, \gamma_j) &= \left(\frac{\alpha_b}{2^{1/\alpha_b+1} \gamma_j^{1/\alpha_b} \Gamma(1/\alpha_b)} \right)^p \left(\prod_{k=1}^p \lambda_{kj} \right)^{1/\alpha_b} \exp \left\{ -\frac{1}{2\gamma_j} \sum_{k=1}^p \lambda_{kj} |B_{kj}|^{\alpha_b} \right\}, \\ \lambda_{kj} &\sim \frac{1}{2} \text{Gamma}(e_{kj,1}, f_{kj,1}) + \frac{1}{2} \text{Gamma}(e_{kj,2}, f_{kj,2}), \\ \alpha_b &\sim \text{Unif}(k_1, k_2), \quad 0 < k_1 \leq 1, \quad k_2 \geq 2, \end{aligned}$$

and the prior for δ_j for $j = 2, \dots, q$ is given by

$$\begin{aligned} \nu(\delta_j|\tau_j, \gamma_j, \alpha_d) &= \left(\frac{\alpha_d}{2^{1/\alpha_d+1} \gamma_j^{1/\alpha_d} \Gamma(1/\alpha_d)} \right)^{j-1} \left(\prod_{k=1}^{j-1} \tau_{j,k} \right)^{1/\alpha_d} \exp \left\{ -\frac{1}{2\gamma_j} \sum_{k=1}^{j-1} \tau_{j,k} |\delta_{j,k}|^{\alpha_d} \right\}, \\ \tau_{j,k} &\sim \frac{1}{2} \text{Gamma}(s_{jk,1}, t_{jk,1}) + \frac{1}{2} \text{Gamma}(s_{jk,2}, t_{jk,2}), \\ \alpha_d &\sim \text{Unif}(k_1, k_2). \end{aligned}$$

Finally, $\gamma_j \sim \text{IG}(a, b)$, $j = 1, \dots, q$.

Define $\gamma = (\gamma_1, \dots, \gamma_q)^\top$ and $\tau = (\tau_2, \tau_3^\top, \dots, \tau_q^\top)^\top$. Let $I\{\cdot\}$ denote the indicator function and $\|\cdot\|_2$ denote the Euclidean norm. The posterior distribution of this model is

characterized by

$$\begin{aligned}
& q(B, \Lambda, \alpha_b, \delta, \gamma, \tau, \alpha_d | Y, X) \\
& \propto \left(\frac{1}{\gamma_1} \right)^{n/2} \exp \left\{ -\frac{1}{2\gamma_1} \|Y^1 - XB^1\|_2^2 \right\} \\
& \quad \cdot \prod_{j=2}^q \left[\left(\frac{1}{\gamma_j} \right)^{n/2} \exp \left\{ -\frac{1}{2\gamma_j} \|Y^j - XB^j - (Y^{1:(j-1)} - XB^{1:(j-1)})\delta_j\|_2^2 \right\} \right] \\
& \quad \cdot \left(\frac{\alpha_b}{2^{1/\alpha_b} \Gamma(1/\alpha_b)} \right)^{pq} \left(\prod_{k=1}^p \prod_{j=1}^q \frac{\lambda_{kj}}{\gamma_j} \right)^{1/\alpha_b} \exp \left\{ -\frac{1}{2} \sum_{k=1}^p \sum_{j=1}^q \frac{\lambda_{kj}}{\gamma_j} |B_{kj}|^{\alpha_b} \right\} \\
& \quad \cdot \prod_{k=1}^p \prod_{j=1}^q \left[\frac{f_{kj,1}^{e_{kj,1}}}{\Gamma(e_{kj,1})} \lambda_{kj}^{e_{kj,1}-1} \exp \{-\lambda_{kj} f_{kj,1}\} + \frac{f_{kj,2}^{e_{kj,2}}}{\Gamma(e_{kj,2})} \lambda_{kj}^{e_{kj,2}-1} \exp \{-\lambda_{kj} f_{kj,2}\} \right] \\
& \quad \cdot I\{k_1 \leq \alpha_b \leq k_2\} I\{k_1 \leq \alpha_d \leq k_2\} \prod_{j=1}^q \left(\frac{1}{\gamma_j} \right)^{a+1} \exp \{-b/\gamma_j\} \\
& \quad \cdot \prod_{j=2}^q \left[\left(\frac{\alpha_d}{2^{1/\alpha_d} \gamma_j^{1/\alpha_d} \Gamma(1/\alpha_d)} \right)^{j-1} \left(\prod_{k=1}^{j-1} \tau_{j,k} \right)^{1/\alpha_d} \exp \left\{ -\frac{1}{2\gamma_j} \sum_{k=1}^{j-1} \tau_{j,k} |\delta_{j,k}|^{\alpha_d} \right\} \right. \\
& \quad \left. \cdot \prod_{k=1}^{j-1} \left(\frac{t_{jk,1}^{s_{jk,1}}}{\Gamma(s_{jk,1})} \tau_{j,k}^{s_{jk,1}-1} \exp \{-\tau_{j,k} t_{jk,1}\} + \frac{t_{jk,2}^{s_{jk,2}}}{\Gamma(s_{jk,2})} \tau_{j,k}^{s_{jk,2}-1} \exp \{-\tau_{j,k} t_{jk,2}\} \right) \right]. \tag{11}
\end{aligned}$$

B.1 Posterior Conditionals

The following posterior conditionals are used to construct the GMCB-MH algorithm.

B.1.1 B_{kj}

Let $B_{(kj)}$ denote the matrix B with B_{kj} removed. The kernel of the posterior conditional for B_{kj} is given by

$$\begin{aligned}
& q(B_{kj} | Y, X, B_{(kj)}, \Lambda, \alpha_b, \delta, \gamma, \tau, \alpha_d) \\
& \propto \exp \left\{ -\frac{1}{2\gamma_j} \lambda_{kj} |B_{kj}|^{\alpha_b} \right\} \exp \left\{ -\frac{1}{2\gamma_1} \|Y^1 - XB^1\|_2^2 \right\} \\
& \quad \cdot \prod_{j=2}^q \exp \left\{ -\frac{1}{2\gamma_j} \|Y^j - XB^j - (Y^{1:(j-1)} - XB^{1:(j-1)})\delta_j\|_2^2 \right\} \\
& = \exp \left\{ -\frac{1}{2\gamma_j} \lambda_{kj} |B_{kj}|^{\alpha_b} \right\} \exp \left\{ -\frac{1}{2} \text{tr}((Y - XB)\Omega(Y - XB)^\top) \right\},
\end{aligned}$$

where in the last line, Ω is a function of δ and γ through the modified Cholesky decomposition in equation (3).

B.1.2 λ_{kj}

Let $\Lambda_{(kj)}$ denote the matrix Λ with λ_{kj} removed. The kernel of the posterior conditional for λ_{kj} is

$$\begin{aligned} & q(\lambda_{kj}|Y, X, B, \Lambda_{(kj)}, \alpha_b, \delta, \gamma, \tau, \alpha_d) \\ & \propto \frac{f_{kj,1}^{e_{kj,1}}}{\Gamma(e_{kj,1})} \lambda_{kj}^{e_{kj,1}+1/\alpha_b-1} \exp \left\{ -\lambda_{kj} \left(f_{kj,1} + \frac{1}{2\gamma_j} |B_{kj}|^{\alpha_b} \right) \right\} \\ & \quad + \frac{f_{kj,2}^{e_{kj,2}}}{\Gamma(e_{kj,2})} \lambda_{kj}^{e_{kj,2}+1/\alpha_b-1} \exp \left\{ -\lambda_{kj} \left(f_{kj,2} + \frac{1}{2\gamma_j} |B_{kj}|^{\alpha_b} \right) \right\}. \end{aligned} \quad (12)$$

Integrating over the right side of equation (12) with respect to λ_{kj} , the normalizing constant is

$$\frac{f_{kj,1}^{e_{kj,1}}}{\Gamma(e_{kj,1})} \frac{\Gamma(e_{kj,1} + 1/\alpha_b)}{\left(f_{kj,1} + \frac{1}{2\gamma_j} |B_{kj}|^{\alpha_b} \right)^{e_{kj,1}+1/\alpha_b}} + \frac{f_{kj,2}^{e_{kj,2}}}{\Gamma(e_{kj,2})} \frac{\Gamma(e_{kj,2} + 1/\alpha_b)}{\left(f_{kj,2} + \frac{1}{2\gamma_j} |B_{kj}|^{\alpha_b} \right)^{e_{kj,2}+1/\alpha_b}}.$$

Let

$$\begin{aligned} w_1 &= \frac{f_{kj,1}^{e_{kj,1}}}{\Gamma(e_{kj,1})} \frac{\Gamma(e_{kj,1} + 1/\alpha_b)}{\left(f_{kj,1} + \frac{1}{2\gamma_j} |B_{kj}|^{\alpha_b} \right)^{e_{kj,1}+1/\alpha_b}} \\ w_2 &= \frac{f_{kj,2}^{e_{kj,2}}}{\Gamma(e_{kj,2})} \frac{\Gamma(e_{kj,2} + 1/\alpha_b)}{\left(f_{kj,2} + \frac{1}{2\gamma_j} |B_{kj}|^{\alpha_b} \right)^{e_{kj,2}+1/\alpha_b}}. \end{aligned}$$

Then the posterior conditional distribution of λ_{kj} is given by

$$\begin{aligned} & q(\lambda_{kj}|Y, X, B, \Lambda_{(kj)}, \alpha_b, \delta, \gamma, \tau, \alpha_d) \\ &= \frac{f_{kj,1}^{e_{kj,1}}/\Gamma(e_{kj,1})}{w_1 + w_2} \lambda_{kj}^{e_{kj,1}+1/\alpha_b-1} \exp \left\{ -\lambda_{kj} \left(f_{kj,1} + \frac{1}{2\gamma_j} |B_{kj}|^{\alpha_b} \right) \right\} \\ & \quad + \frac{f_{kj,2}^{e_{kj,2}}/\Gamma(e_{kj,2})}{w_1 + w_2} \lambda_{kj}^{e_{kj,2}+1/\alpha_b-1} \exp \left\{ -\lambda_{kj} \left(f_{kj,2} + \frac{1}{2\gamma_j} |B_{kj}|^{\alpha_b} \right) \right\}. \end{aligned}$$

Therefore,

$$\begin{aligned} \lambda_{kj}|Y, X, B, \Lambda_{(kj)}, \alpha_b, \delta, \gamma, \tau, \alpha_d &\sim \frac{w_1}{w_1 + w_2} \text{Gamma} \left(e_{kj,1} + \frac{1}{\alpha_b}, f_{kj,1} + \frac{1}{2\gamma_j} |B_{kj}|^{\alpha_b} \right) \\ & \quad + \frac{w_2}{w_1 + w_2} \text{Gamma} \left(e_{kj,2} + \frac{1}{\alpha_b}, f_{kj,2} + \frac{1}{2\gamma_j} |B_{kj}|^{\alpha_b} \right). \end{aligned}$$

B.1.3 $\delta_{j,k}$

Let $\delta_{(j,k)}$ denote the vector δ with $\delta_{j,k}$ removed. The kernel of the posterior conditional for $\delta_{j,k}$ is given by

$$q(\delta_{j,k}|Y, X, B, \Lambda, \alpha_b, \delta_{(j,k)}, \gamma, \tau, \alpha_d) \\ \propto \exp \left\{ -\frac{1}{2\gamma_j} \tau_{j,k} |\delta_{j,k}|^{\alpha_d} \right\} \exp \left\{ -\frac{1}{2\gamma_j} \|Y^j - XB^j - (Y^{1:(j-1)} - XB^{1:(j-1)})\delta_j\|_2^2 \right\}.$$

B.1.4 γ

Let $\gamma_{(j)}$ denote the vector γ with γ_j removed. The kernel for the posterior conditional for γ_1 is given by

$$q(\gamma_1|Y, X, B, \Lambda, \alpha_b, \delta, \tau, \gamma_{(1)}, \alpha_d) \\ \propto \left(\frac{1}{\gamma_1} \right)^{\frac{n}{2} + \frac{p}{\alpha_b} + a + 1} \exp \left\{ -\frac{1}{\gamma_1} \left(\frac{1}{2} \|Y^1 - XB^1\|_2^2 + \frac{1}{2} \sum_{k=1}^p \lambda_{k1} |B_{k1}|^{\alpha_b} + b \right) \right\},$$

so

$$\gamma_1|Y, X, B, \Lambda, \alpha_b, \delta, \tau, \gamma_{(1)}, \alpha_d \sim \text{Gamma} \left(\frac{n}{2} + \frac{p}{\alpha_b} + a, \frac{1}{2} \|Y^1 - XB^1\|_2^2 + \frac{1}{2} \sum_{k=1}^p \lambda_{k1} |B_{k1}|^{\alpha_b} + b \right).$$

The kernel for the posterior conditional for γ_j , $j = 2, \dots, q$ is given by

$$q(\gamma_j|Y, X, B, \Lambda, \alpha_b, \delta, \tau, \gamma_{(j)}, \alpha_d) \\ \propto \left(\frac{1}{\gamma_j} \right)^{\frac{n}{2} + \frac{j-1}{\alpha_d} + \frac{p}{\alpha_b} + a + 1} \cdot \exp \left\{ -\frac{1}{\gamma_j} \left(\frac{1}{2} \|Y^j - XB^j - (Y^{1:(j-1)} - XB^{1:(j-1)})\delta_j\|_2^2 \right. \right. \\ \left. \left. + \frac{1}{2} \sum_{k=1}^{j-1} \tau_{j,k} |\delta_{j,k}|^{\alpha_d} + \frac{1}{2} \sum_{k=1}^p \lambda_{kj} |B_{kj}|^{\alpha_b} + b \right) \right\},$$

so

$$\gamma_j|Y, X, B, \Lambda, \alpha_b, \delta, \tau, \gamma_{(1)}, \alpha_d \\ \sim \text{Gamma} \left(\frac{n}{2} + \frac{j-1}{\alpha_d} + \frac{p}{\alpha_b} + a, \right. \\ \left. \frac{1}{2} \|Y^j - XB^j - (Y^{1:(j-1)} - XB^{1:(j-1)})\delta_j\|_2^2 + \frac{1}{2} \sum_{k=1}^{j-1} \tau_{j,k} |\delta_{j,k}|^{\alpha_d} \right. \\ \left. + \frac{1}{2} \sum_{k=1}^p \lambda_{kj} |B_{kj}|^{\alpha_b} + b \right).$$

B.1.5 $\tau_{j,k}$

Let $\tau_{(j,k)}$ denote the vector τ with $\tau_{j,k}$ removed. The kernel for the posterior conditional for $\tau_{j,k}$ is given by

$$\begin{aligned} & q(\tau_{j,k}|Y, X, B, \Lambda, \alpha_b, \delta, \gamma, \tau_{(j,k)}, \alpha_d) \\ & \propto \frac{t_{jk,1}^{s_{jk,1}}}{\Gamma(s_{jk,1})} \tau_{j,k}^{s_{jk,1}+1/\alpha_d-1} \exp \left\{ -\tau_{j,k} \left(t_{jk,1} + \frac{1}{2\gamma_j} |\delta_{j,k}|^{\alpha_d} \right) \right\} \\ & \quad + \frac{t_{jk,2}^{s_{jk,2}}}{\Gamma(s_{jk,2})} \tau_{j,k}^{s_{jk,2}+1/\alpha_d-1} \exp \left\{ -\tau_{j,k} \left(t_{jk,2} + \frac{1}{2\gamma_j} |\delta_{j,k}|^{\alpha_d} \right) \right\}. \end{aligned} \quad (13)$$

Integrating over the right side of equation (13) with respect to $\tau_{j,k}$, the normalizing constant is

$$\frac{t_{jk,1}^{s_{jk,1}}}{\Gamma(s_{jk,1})} \frac{\Gamma(s_{jk,1} + 1/\alpha_d)}{\left(t_{jk,1} + \frac{1}{2\gamma_j} |\delta_{j,k}|^{\alpha_d} \right)^{s_{jk,1}+1/\alpha_d}} + \frac{t_{jk,2}^{s_{jk,2}}}{\Gamma(s_{jk,2})} \frac{\Gamma(s_{jk,2} + 1/\alpha_d)}{\left(t_{jk,2} + \frac{1}{2\gamma_j} |\delta_{j,k}|^{\alpha_d} \right)^{s_{jk,2}+1/\alpha_d}}.$$

Let

$$\begin{aligned} d_1 &= \frac{t_{jk,1}^{s_{jk,1}}}{\Gamma(s_{jk,1})} \frac{\Gamma(s_{jk,1} + 1/\alpha_d)}{\left(t_{jk,1} + \frac{1}{2\gamma_j} |\delta_{j,k}|^{\alpha_d} \right)^{s_{jk,1}+1/\alpha_d}} \\ d_2 &= \frac{t_{jk,2}^{s_{jk,2}}}{\Gamma(s_{jk,2})} \frac{\Gamma(s_{jk,2} + 1/\alpha_d)}{\left(t_{jk,2} + \frac{1}{2\gamma_j} |\delta_{j,k}|^{\alpha_d} \right)^{s_{jk,2}+1/\alpha_d}}. \end{aligned}$$

Then the posterior conditional distribution of $\tau_{j,k}$ is given by

$$\begin{aligned} & q(\tau_{j,k}|Y, X, B, \Lambda, \alpha_b, \delta, \gamma, \tau_{(j,k)}, \alpha_d) \\ & = \frac{t_{jk,1}^{s_{jk,1}}/\Gamma(s_{jk,1})}{d_1 + d_2} \tau_{j,k}^{s_{jk,1}+1/\alpha_d-1} \exp \left\{ -\tau_{j,k} \left(t_{jk,1} + \frac{1}{2\gamma_j} |\delta_{j,k}|^{\alpha_d} \right) \right\} \\ & \quad + \frac{t_{jk,2}^{s_{jk,2}}/\Gamma(s_{jk,2})}{d_1 + d_2} \tau_{j,k}^{s_{jk,2}+1/\alpha_d-1} \exp \left\{ -\tau_{j,k} \left(t_{jk,2} + \frac{1}{2\gamma_j} |\delta_{j,k}|^{\alpha_d} \right) \right\}. \end{aligned}$$

Therefore,

$$\begin{aligned} \tau_{j,k}|Y, X, B, \Lambda, \alpha_b, \delta, \gamma, \tau_{(j,k)}, \alpha_d & \sim \frac{d_1}{d_1 + d_2} \text{Gamma} \left(s_{jk,1} + \frac{1}{\alpha_d}, t_{jk,1} + \frac{1}{2\gamma_j} |\delta_{j,k}|^{\alpha_d} \right) \\ & \quad + \frac{d_2}{d_1 + d_2} \text{Gamma} \left(s_{jk,2} + \frac{1}{\alpha_d}, t_{jk,2} + \frac{1}{2\gamma_j} |\delta_{j,k}|^{\alpha_d} \right). \end{aligned}$$

B.1.6 α_b

The kernel of the posterior conditional for α_b is given by

$$q(\alpha_b|Y, X, B, \Lambda, \delta, \gamma, \tau, \alpha_d) \propto \left(\frac{\alpha_b}{2^{1/\alpha_b} \Gamma(1/\alpha_b)} \right)^{pq} \left(\prod_{k=1}^p \prod_{j=1}^q \frac{\lambda_{kj}}{\gamma_j} \right)^{1/\alpha_b} \exp \left\{ -\frac{1}{2} \sum_{k=1}^p \sum_{j=1}^q \frac{\lambda_{kj}}{\gamma_j} |B_{kj}|^{\alpha_b} \right\} I\{k_1 \leq \alpha_b \leq k_2\}.$$

B.1.7 α_d

The kernel of the posterior conditional for α_d is given by

$$q(\alpha_d|Y, X, B, \Lambda, \alpha_b, \delta, \gamma, \tau) \propto \prod_{j=2}^q \left(\frac{\alpha_d}{2^{1/\alpha_d} \gamma_j^{1/\alpha_d} \Gamma(1/\alpha_d)} \right)^{j-1} \left(\prod_{k=1}^{j-1} \tau_{j,k} \right)^{1/\alpha_d} \exp \left\{ -\frac{1}{2\gamma_j} \sum_{k=1}^{j-1} \tau_{j,k} |\delta_{j,k}|^{\alpha_d} \right\} I\{k_1 \leq \alpha_d \leq k_2\}.$$

B.2 Posterior Conditionals under SMN

The parameters B and δ can be easily sampled under a SMN representation. For the exponential power distribution with density proportional to $\exp\{-|x|^\alpha\}$, the mixing density in terms of the standard deviation σ is $h(\sigma) \propto \sigma^{-2} p_{\alpha/2}(\sigma^{-2})$, where $p_{\alpha/2}$ is the density of a positive stable distribution with index $\alpha/2 < 1$ (West, 1987). The mixing density in terms of the precision $\omega = 1/\sigma^2$ is then $g(\omega) \propto \omega^{-1/2} p_{\alpha/2}(\omega)$.

B.2.1 B_{kj}

Let ω_{kj} denote the latent variable associated with B_{kj} . Under the SMN representation, the prior on B_{kj} is given by

$$B_{kj}|\omega_{kj}, \lambda_{kj}, \gamma_j, \alpha_b \sim N \left(0, \frac{1}{\omega_{kj}} \left(\frac{2\gamma_j}{\lambda_{kj}} \right)^{2/\alpha_b} \right),$$

$$g(\omega_{kj}|\alpha_b) \propto \omega_{kj}^{-1/2} p_{\alpha_b/2}(\omega_{kj}).$$

Define $\omega \in \mathbb{R}^{p \times q}$ to be the matrix of latent variables associated with B . Then

$$q(B, \omega|Y, X, \Lambda, \alpha_b, \delta, \gamma, \tau, \alpha_d) \propto \exp \left\{ -\frac{1}{2} \text{tr}((Y - XB)\Omega(Y - XB)^\top) \right\} \cdot \prod_{k=1}^p \prod_{j=1}^q \left[\left(\frac{\omega_{kj} \lambda_{kj}^{2/\alpha_b}}{(2\gamma_j)^{2/\alpha_b}} \right)^{1/2} \exp \left\{ -\frac{\omega_{kj} \lambda_{kj}^{2/\alpha_b}}{2(2\gamma_j)^{2/\alpha_b}} B_{kj}^2 \right\} \omega_{kj}^{-1/2} p_{\alpha_b/2}(\omega_{kj}) \right]. \quad (14)$$

Let $\omega_{(kj)}$ denote the matrix ω with ω_{kj} removed. The posterior conditional for ω_{kj} associated with equation (14) is given by

$$q(\omega_{kj}|Y, X, B, \Lambda, \alpha_b, \delta, \gamma, \tau, \alpha_d, \omega_{(kj)}) \propto \exp \left\{ -\frac{\lambda_{kj}^{2/\alpha_b} B_{kj}^2}{2(2\gamma_j)^{2/\alpha_b}} \omega_{kj} \right\} p_{\alpha_b/2}(\omega_{kj}),$$

which is an exponentially tilted positive stable distribution. The algorithm described in Devroye (2009) and a modified version of the implementation in the R package copula (Hofert et al., 2020) is used to sample ω_{kj} .

Let \otimes and \odot denote the Kronecker and Hadamard products, respectively. Define $[\gamma]_p$ to be the vector γ with each of its elements repeated p times and the $pq \times pq$ matrix Δ to be

$$\Delta = \text{diag}[\text{vec}(\omega) \odot \text{vec}(\Lambda)^{2/\alpha_b}] \left(\text{diag}[(2[\gamma]_p)^{2/\alpha_b}] \right)^{-1}.$$

Then the posterior conditional for B associated with equation (14) is given by

$$\begin{aligned} & q(B|Y, X, \Lambda, \alpha_b, \delta, \gamma, \tau, \alpha_d, \omega) \\ & \propto \exp \left\{ -\frac{1}{2} \text{tr}((Y - XB)\Omega(Y - XB)^\top) \right\} \prod_{k=1}^p \prod_{j=1}^q \exp \left\{ -\frac{\omega_{kj} \lambda_{kj}^{2/\alpha_b}}{2(2\gamma_j)^{2/\alpha_b}} B_{kj}^2 \right\} \\ & = \exp \left\{ -\frac{1}{2} \text{tr}((Y - XB)\Omega(Y - XB)^\top) \right\} \exp \left\{ -\frac{1}{2} \text{vec}(B)^\top \Delta \text{vec}(B) \right\}. \end{aligned} \quad (15)$$

When $p < n$, let $\hat{B} = (X^\top X)^{-1} X^\top Y$. Define $\Theta = \Omega^{-1} \otimes (X^\top X)^{-1}$ and $\Phi = \Theta^{-1} + \Delta$. Then equation (15) is proportional to

$$\begin{aligned} & \exp \left\{ -\frac{1}{2} \text{tr}(X^\top X(B - \hat{B})\Omega(B - \hat{B})^\top) \right\} \exp \left\{ -\frac{1}{2} \text{vec}(B)^\top \Delta \text{vec}(B) \right\} \\ & = \exp \left\{ -\frac{1}{2} [\text{vec}(B) - \text{vec}(\hat{B})]^\top \Theta^{-1} [\text{vec}(B) - \text{vec}(\hat{B})] \right\} \exp \left\{ -\frac{1}{2} \text{vec}(B)^\top \Delta \text{vec}(B) \right\} \\ & \propto \exp \left\{ -\frac{1}{2} \left(\text{vec}(B)^\top \Phi \text{vec}(B) - 2 \text{vec}(\hat{B})^\top \Theta^{-1} \text{vec}(B) \right) \right\} \\ & = \exp \left\{ -\frac{1}{2} \left(\text{vec}(B)^\top \Phi \text{vec}(B) - 2 \text{vec}(\hat{B})^\top \Theta^{-1} \Phi^{-1} \Phi \text{vec}(B) \right) \right\}, \end{aligned}$$

so

$$\text{vec}(B)|Y, X, \text{vec}(\Lambda), \alpha_b, \delta, \gamma, \tau, \alpha_d, \text{vec}(\omega) \sim N_{pq} \left(\Phi^{-1} \Theta^{-1} \text{vec}(\hat{B}), \Phi^{-1} \right). \quad (16)$$

To show that equation (15) is a normal distribution even when $(X^\top X)^{-1}$ does not exist requires a variable transformation. Let $X = UCV^\top$ denote the SVD of X , where

$U \in \mathbb{R}^{n \times n}$ and $V \in \mathbb{R}^{p \times p}$ are orthonormal and $C \in \mathbb{R}^{n \times p}$. Let $r = \text{rank}(X)$. Define

$$\begin{aligned} w &= \max(p - r, 0) \\ z &= \max(n - r, 0), \end{aligned}$$

and let $\psi \in \mathbb{R}^{r \times r}$ be the diagonal matrix with diagonal elements the positive singular values of X . Then

$$C = \begin{pmatrix} \psi & 0_{r \times w} \\ 0_{z \times r} & 0_{z \times w} \end{pmatrix}.$$

Define $\eta = V^\top B T^\top$. The Jacobian of this transformation is a constant with respect to η , and equation (15) can be rewritten as

$$\begin{aligned} & q(\eta|Y, X, \Lambda, \alpha_b, \delta, \gamma, \tau, \alpha_d, \omega) \\ & \propto \exp \left\{ -\frac{1}{2} \left[\text{tr}[D^{-1}(-TY^\top UC\eta - \eta^\top C^\top U^\top Y T^\top + \eta^\top C^\top C\eta)] \right. \right. \\ & \quad \left. \left. + \text{vec}(V\eta(T^{-1})^\top)^\top \Delta \text{vec}(V\eta(T^{-1})^\top) \right] \right\} \\ & = \exp \left\{ -\frac{1}{2} \left[-2 \text{tr}(D^{-1}TY^\top UC\eta) + \text{tr}(D^{-1}\eta^\top C^\top C\eta) \right. \right. \\ & \quad \left. \left. + \text{vec}(\eta)^\top (T^{-1} \otimes V)^\top \Delta (T^{-1} \otimes V) \text{vec}(\eta) \right] \right\} \\ & = \exp \left\{ -\frac{1}{2} \left[-2 \text{vec}(C^\top U^\top Y T^\top D^{-1})^\top \text{vec}(\eta) + \text{vec}(C\eta D^{-1/2})^\top \text{vec}(C\eta D^{-1/2}) \right. \right. \\ & \quad \left. \left. + \text{vec}(\eta)^\top (T^{-1} \otimes V)^\top \Delta (T^{-1} \otimes V) \text{vec}(\eta) \right] \right\} \\ & = \exp \left\{ -\frac{1}{2} \left[-2 \text{vec}(C^\top U^\top Y T^\top D^{-1})^\top \text{vec}(\eta) + \text{vec}(\eta)^\top (D^{-1/2} \otimes C)^\top (D^{-1/2} \otimes C) \text{vec}(\eta) \right. \right. \\ & \quad \left. \left. + \text{vec}(\eta)^\top (T^{-1} \otimes V)^\top \Delta (T^{-1} \otimes V) \text{vec}(\eta) \right] \right\} \\ & = \exp \left\{ -\frac{1}{2} \left[-2 \text{vec}(C^\top U^\top Y T^\top D^{-1})^\top \text{vec}(\eta) + \text{vec}(\eta)^\top (D^{-1} \otimes C^\top C) \text{vec}(\eta) \right. \right. \\ & \quad \left. \left. + \text{vec}(\eta)^\top (T^{-1} \otimes V)^\top \Delta (T^{-1} \otimes V) \text{vec}(\eta) \right] \right\} \\ & = \exp \left\{ -\frac{1}{2} \left[-2 \text{vec}(C^\top U^\top Y T^\top D^{-1})^\top \text{vec}(\eta) \right. \right. \\ & \quad \left. \left. + \text{vec}(\eta)^\top [(D^{-1} \otimes C^\top C) + (T^{-1} \otimes V)^\top \Delta (T^{-1} \otimes V)] \text{vec}(\eta) \right] \right\}. \end{aligned}$$

Define $\Theta = [(D^{-1} \otimes C^\top C) + (T^{-1} \otimes V)^\top \Delta (T^{-1} \otimes V)]^{-1}$. Then

$$\text{vec}(\eta)|Y, X, \text{vec}(\Lambda), \alpha_b, \delta, \gamma, \tau, \alpha_d, \text{vec}(\omega) \sim N_{pq}(\Theta \text{vec}(C^\top U^\top Y T^\top D^{-1}), \Theta). \quad (17)$$

For $p < n$, B is sampled directly using equation (16). For $p \geq n$, B is obtained by first sampling from equation (17) using the algorithm by [Bhattacharya et al. \(2016\)](#):

1. Sample $u \sim N(0, (T \otimes V^\top) \Delta^{-1} (T^\top \otimes V))$ and $e \sim N(0, I_{nq})$ independently.

2. Set $v = (D^{-1/2} \otimes C)u + e$.

3. Solve for w in

$$[(D^{-1/2}T \otimes CV^\top)\Delta^{-1}(T^\top D^{-1/2} \otimes VC^\top) + I_{nq}]w = \text{vec}(U^\top YT^\top D^{-1/2}) - v.$$

4. Set $\text{vec}(\eta) = u + (T \otimes V^\top)\Delta^{-1}(T^\top D^{-1/2} \otimes VC^\top)w$.

B.2.2 δ_j

Let $\epsilon_{j,k}$ be the latent variable associated with $\delta_{j,k}$. The prior on $\delta_{j,k}$ can be represented as

$$\begin{aligned} \delta_{j,k} | \epsilon_{j,k}, \tau_{j,k}, \gamma_j, \alpha_d &\sim N \left(0, \frac{1}{\epsilon_{j,k}} \left(\frac{2\gamma_j}{\tau_{j,k}} \right)^{2/\alpha_d} \right), \\ g(\epsilon_{j,k} | \alpha_d) &\propto \epsilon_{j,k}^{-1/2} p_{\alpha_d/2}(\epsilon_{j,k}). \end{aligned}$$

Define $\epsilon \in \mathbb{R}^{q(q-1)/2}$ to be the vector of latent variables associated with δ . Then

$$\begin{aligned} &q(\delta, \epsilon | Y, X, B, \Lambda, \alpha_b, \gamma, \tau, \alpha_d) \\ &\propto \prod_{j=2}^q \left[\exp \left\{ -\frac{1}{2\gamma_j} \|Y^j - XB^j - (Y^{1:(j-1)} - XB^{1:(j-1)})\delta_j\|_2^2 \right\} \right. \\ &\quad \left. \cdot \prod_{k=1}^{j-1} \left(\frac{\epsilon_{j,k} \tau_{j,k}^{2/\alpha_d}}{(2\gamma_j)^{2/\alpha_d}} \right)^{1/2} \exp \left\{ -\frac{\epsilon_{j,k} \tau_{j,k}^{2/\alpha_d}}{2(2\gamma_j)^{2/\alpha_d}} \delta_{j,k}^2 \right\} \epsilon_{j,k}^{-1/2} p_{\alpha_d/2}(\epsilon_{j,k}) \right]. \end{aligned} \quad (18)$$

Let $\epsilon_{(j,k)}$ denote the vector ϵ with $\epsilon_{j,k}$ removed. The posterior conditional for $\epsilon_{j,k}$ corresponding to equation (18) is

$$q(\epsilon_{j,k} | Y, X, B, \Lambda, \alpha_b, \delta, \gamma, \tau, \alpha_d, \epsilon_{(j,k)}) \propto \exp \left\{ -\frac{\tau_{j,k}^{2/\alpha_d} \delta_{j,k}^2}{2(2\gamma_j)^{2/\alpha_d}} \epsilon_{j,k} \right\} p_{\alpha_d/2}(\epsilon_{j,k}).$$

This is an exponentially tilted positive stable distribution and can be sampled from using the algorithm described in [Devroye \(2009\)](#).

Let $Z_j = Y^j - XB^j$, $W_j = Y^{1:(j-1)} - XB^{1:(j-1)}$, $\tau_j = (\tau_{j,1}, \dots, \tau_{j,j-1})^\top$, and $\epsilon_j = (\epsilon_{j,1}, \dots, \epsilon_{j,j-1})^\top$. Define the $(j-1) \times (j-1)$ matrix Ψ_j to be $\Psi_j = \text{diag}[(\epsilon_j \odot \tau_j^{2/\alpha_d}) / (2\gamma_j)^{2/\alpha_d}]$, and let $\delta_{(j)}$ denote the vector δ with δ_j removed. Then the posterior conditional for δ_j

corresponding to equation (18) is

$$\begin{aligned}
& q(\delta_j | Y, X, B, \Lambda, \alpha_b, \delta_{(j)}, \gamma, \tau, \alpha_d, \epsilon) \\
& \propto \exp \left\{ -\frac{1}{2\gamma_j} \|Z_j - W_j \delta_j\|_2^2 \right\} \exp \left\{ -\frac{1}{2} \delta_j^\top \Psi_j \delta_j \right\} \\
& \propto \exp \left\{ -\frac{1}{2\gamma_j} (\delta_j^\top W_j^\top W_j \delta_j - 2Z_j^\top W_j \delta_j + \delta_j^\top (\gamma_j \Psi_j) \delta_j) \right\} \\
& = \exp \left\{ -\frac{1}{2\gamma_j} (\delta_j^\top (W_j^\top W_j + \gamma_j \Psi_j) \delta_j - 2Z_j^\top W_j (W_j^\top W_j + \gamma_j \Psi_j)^{-1} (W_j^\top W_j + \gamma_j \Psi_j) \delta_j) \right\},
\end{aligned}$$

so

$$\delta_j | Y, X, B, \Lambda, \alpha_b, \delta_{(j)}, \gamma, \tau, \alpha_d, \epsilon \sim N_{j-1} \left((W_j^\top W_j + \gamma_j \Psi_j)^{-1} W_j^\top Z_j, \gamma_j (W_j^\top W_j + \gamma_j \Psi_j)^{-1} \right).$$

Recall that $j = 2, \dots, q$. For $j \leq n$, δ_j is sampled directly. For $j > n$, the algorithm proposed by [Bhattacharya et al. \(2016\)](#) is used:

1. Sample $u \sim N(0, \Psi_j^{-1})$ and $e \sim N(0, I_n)$ independently.
2. Set $v = \frac{1}{\sqrt{\gamma_j}} W_j u + e$.
3. Solve for w in $(\frac{1}{\gamma_j} W_j \Psi_j^{-1} W_j^\top + I_n) w = \frac{1}{\sqrt{\gamma_j}} Z_j - v$.
4. Set $\delta_j = u + \frac{1}{\sqrt{\gamma_j}} \Psi_j^{-1} W_j^\top w$.

C Additional autocorrelation plots

Figures 8 and 9 display the autocorrelation plots for randomly selected elements of B and δ in Scenarios 2 and 3 as described in 5. These plots are typical of what was observed for B and δ in each scenario.

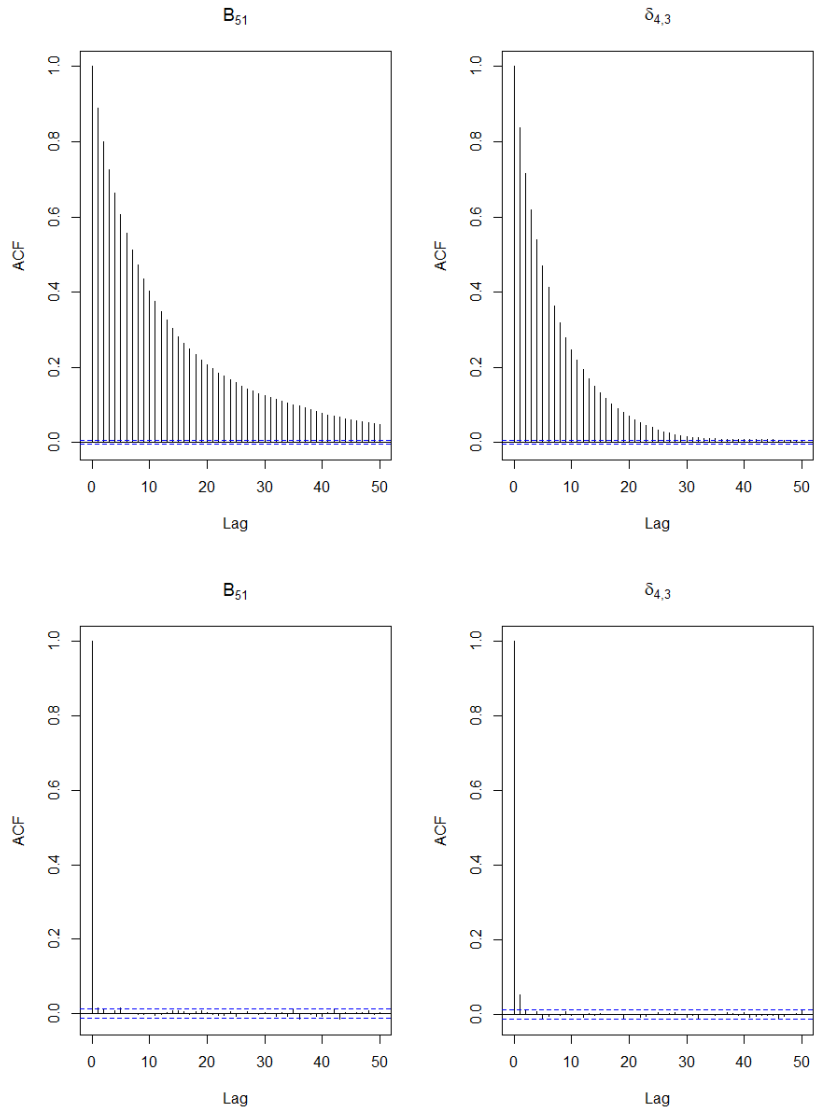


Figure 8: Autocorrelation plots for randomly selected elements of B and δ in Scenario 2 in Section 5. The top plots correspond to GMCB-MH and the bottom plots correspond to GMCB-SMN.

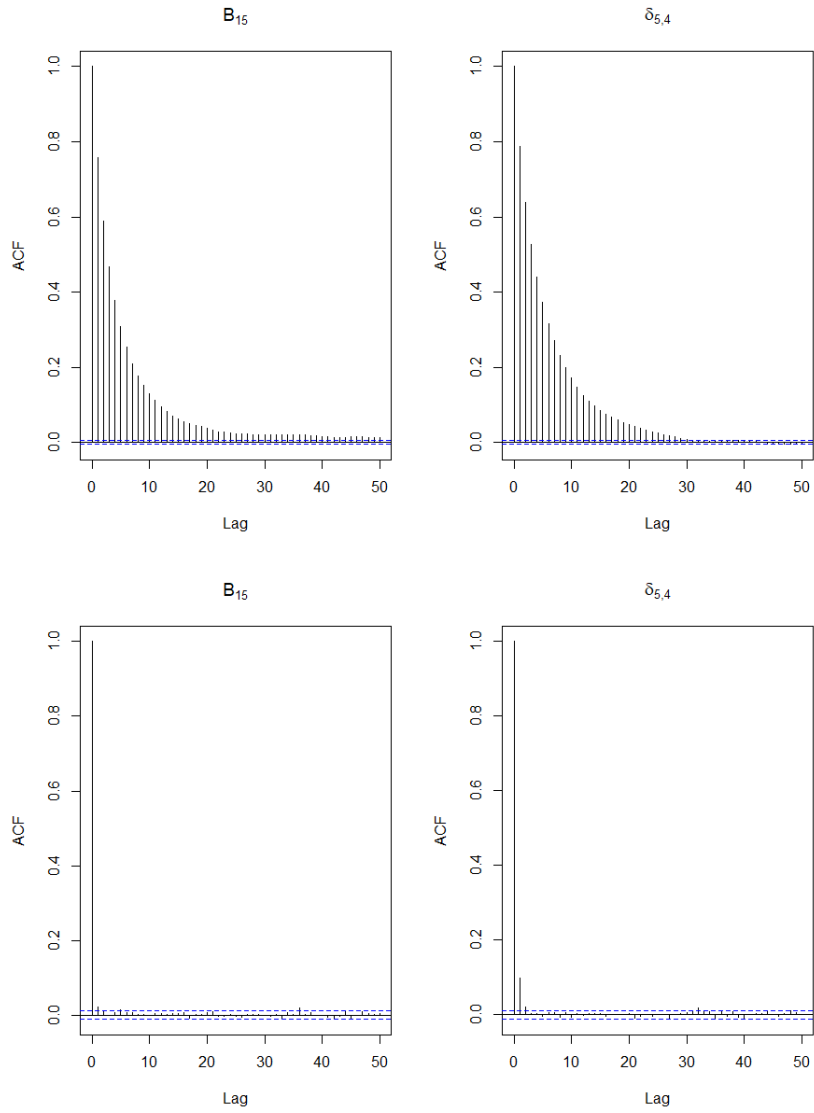


Figure 9: Autocorrelation plots for randomly selected elements of B and δ in Scenario 3 in Section 5. The top plots correspond to GMCB-MH and the bottom plots correspond to GMCB-SMN.

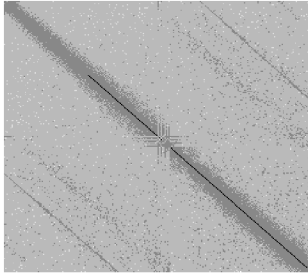
D WISP Survey Example Sensitivity Analysis

Table 6 gives the hyperparameter combinations considered in the sensitivity analysis. Recall that C_0 denotes the class of spectra with no emission lines and C_1 denotes the class of spectra with emission lines. Figures 10 and 11 compare $\hat{\Omega}_F$ and $\hat{\Omega}_S$ under each of these priors with the estimates in Section 6 for C_0 and C_1 , respectively. As shown in the figures, there is little qualitative difference in the estimates, and all eight matrices for C_0 exhibit the band patterns discussed in Section 6. All results are based on 1e6 iterations of the GMCB-SMN algorithm.

Table 6: Priors considered in the sensitivity analysis.

Model	Regularization Parameters	Penalty Parameters	γ
1	$1/2[\text{Gamma}(0.1, 1) + \text{Gamma}(2, 0.1)]$	Unif(0.5,2)	IG(1e-3, 1e-3)
2	$1/2[\text{Gamma}(1, 1) + \text{Gamma}(40, 0.5)]$	Unif(1,2)	empirical
3	$1/2[\text{Gamma}(1, 1) + \text{Gamma}(40, 0.5)]$	Unif(1,2)	IG(1e-3, 1e-3)

GMCB-SMN $\hat{\Omega}_F$



GMCB-SMN $\hat{\Omega}_S$

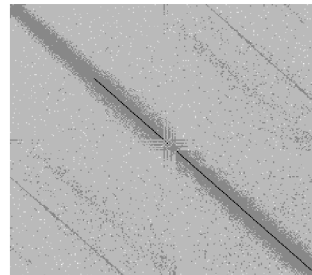
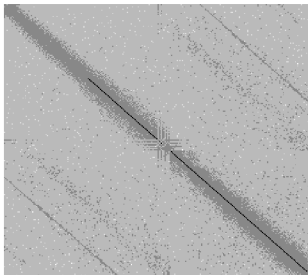
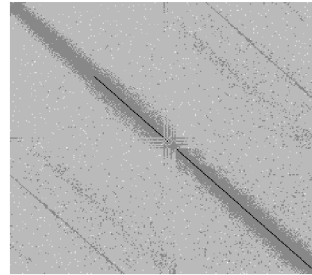
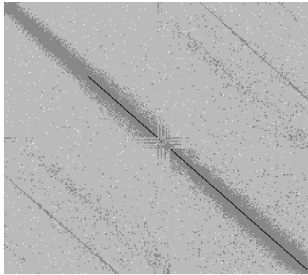
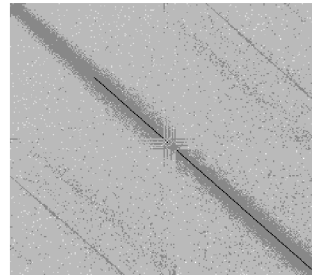
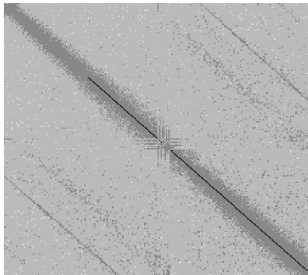
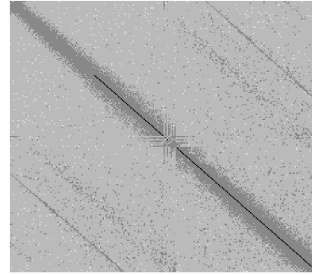
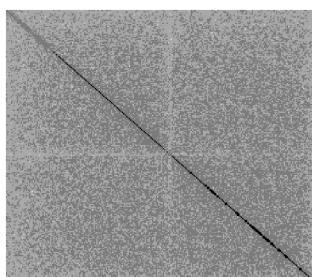


Figure 10: Log of the absolute value of entries of the estimated precision matrices for C_0 , where darker colors correspond to larger values for the model in Section 6 (top row), Model 1 (second row), Model 2 (third row), and Model 3 (bottom row).

GMCB-SMN $\hat{\Omega}_F$



GMCB-SMN $\hat{\Omega}_S$

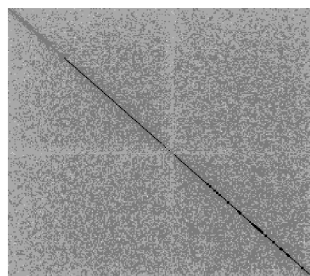
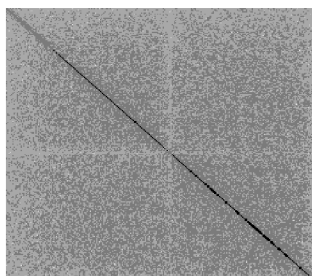
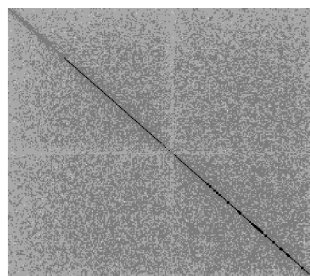
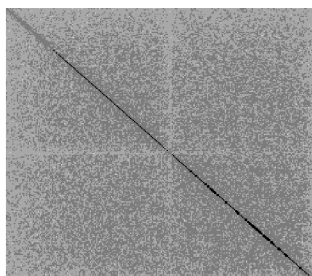
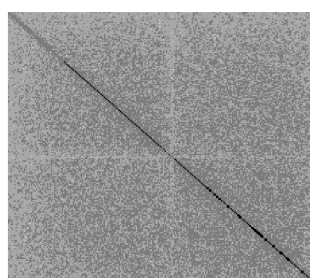
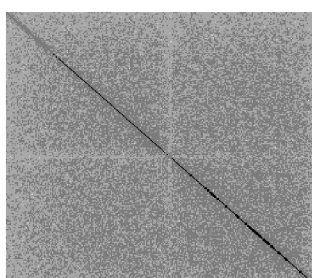
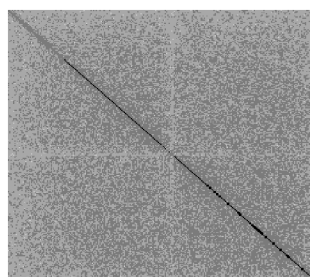


Figure 11: Log of the absolute value of entries of the estimated precision matrices for C_1 , where darker colors correspond to larger values for the model in Section 6 (top row), Model 1 (second row), Model 2 (third row), and Model 3 (bottom row).